
NUMERICAL RECONSTRUCTION OF THE KINETIC CHEMOTAXIS KERNEL FROM MACROSCOPIC MEASUREMENT, WELLPOSEDNESS AND ILLPOSEDNESS

PREPRINT

 **Kathrin Hellmuth**

Department of Mathematics
University of Würzburg
97074 Würzburg, Germany
kathrin.hellmuth@uni-wuerzburg.de

 **Christian Klingenberg**

Department of Mathematics
University of Würzburg
97074 Würzburg, Germany
klingen@mathematik.uni-wuerzburg.de

 **Qin Li**

Department of Mathematics
University of Wisconsin-Madison
Madison, WI, 53706, USA
qinli@math.wisc.edu

Min Tang

School of Mathematics and Institute of Natural Sciences, MOE-LSC
Shanghai Jiaotong University
Shanghai, 200240, China
tangmin@sjtu.edu.cn

October 22, 2021

ABSTRACT

Directed bacterial motion due to external stimuli (chemotaxis) can, on the mesoscopic phase space, be described by a velocity change parameter K . The numerical reconstruction for K from experimental data provides useful insights and plays a crucial role in model fitting, verification and prediction. In this article, the PDE-constrained optimization framework is deployed to perform the reconstruction of K from velocity-averaged, localized data taken in the interior of a 1D domain. Depending on the data preparation and experimental setup, this problem can either be well- or ill-posed. We analyze these situations, and propose a very specific design that guarantees local convergence. The design is adapted to the discretization of K and decouples the reconstruction of local values into smaller cell problem, opening up opportunities for parallelization. We further provide numerical evidence as a showcase for the theoretical results.

Keywords inverse problems in PDEs; numerical methods for inverse problems with PDEs; PDE-constrained optimization; kinetic chemotaxis equation; numerical analysis; well- and ill-posedness; mathematical biology

Funding

K.H. acknowledges support by the German Academic Scholarship Foundation (Studienstiftung des deutschen Volkes) and the Marianne-Plehn-Program.

Q.L. is partially supported by Vice Chancellor for Research and Graduate Education, DMS-2308440 and ONR-N000142112140.

M.T. is partially supported by the Strategic Priority Research Program of Chinese Academy of Sciences, XDA25010401 and NSFC12031013.

1 Introduction

Kinetic chemotaxis equation is one of the classical equations describing the collective behavior of bacteria motion. Presented on the phase space, the equation describes the “run-and-tumble” bacteria motion. The solution $f(t, x, v)$

represents the density of bacteria at any given time t for any location x moving with velocity v . Since it contains more detailed phase-space information, compared to macroscopic models at the population level, such as the Keller Segel model, the equation has the greater potential to capture the fine motion of the bacteria. Indeed, it is observed that the dynamics predicted by the model is in high agreement with real measurements, see Berg [1993], Emako et al. [2016], Saragosti et al. [2011, 2010].

It is noteworthy that these comparisons are conducted in the forward-simulation setting. Guesses are made about parameters, and simulations are run to be compared with experimental measurements. To fully reveal the bacteria's motion and its interaction with the environment, inverse perspectives have to be taken. The measurement data can be at the individual or the population level, i.e., biophysicists can use a high-resolution camera and trace each single bacterium for a long time or they can take photos and record the evolution of the density of bacteria on a cell cultural dish. These collected data should be used to unveil the true interaction between particles Li et al. [2019]. This framework necessitates the application of numerical inversion algorithms. To be specific, we frame this problem into a PDE-constrained optimization and study the well-posedness and the ill-posedness of the numerical reconstruction when different types of initial condition and measurement schemes are provided.

As more first-principle based physics get involved in applications, kinetic models are becoming more important in scientific domains, see modeling of neutrons Davison and Sykes [1958], photons or electrons Rybicki and Lightman [1986] and rarefied gas Cercignani [2012]. The applications on biological and social science have also been put forward in Othmer et al. [1988] for cell motion, in Taylor-King et al. [2014] for animal (birds) migration or in Albi et al. [2023], Carrillo et al. [2009], Chu et al. [2022], Motsch and Tadmor [2014], Toscani [2006] for opinion formation. In most, if not all of these models, parameters are included to characterize the interactions between agents or with the media. The applications in which the interactions are hard to be measured experimentally naturally prompts the use of inverse solvers.

The most prominent application of inverse problem confined to the domain of kinetic-equation governed systems is optical tomography from medical imaging, where non-intrusive boundary data maps out the relation between optical properties of interior bio-tissue and the measured light intensity on the surface of the domain. Mathematically the problem is framed to evaluate the richness of data in the albedo operator. Singular decomposition is deployed as a specific mathematical technique to conduct such investigation Bal et al. [2008], Choulli and Stefanov [1996], Lai et al. [2019], Li and Sun [2020], and these studies have their numerical counterparts in Arridge and Schotland [2009], Chen et al. [2018], Egger and Schlottbom [2013], Prieto and Dorn [2016], Ren [2010], just to mention a few references.

Since tracing every single bacterium is much more difficult than measuring the density evolution and is sometimes not possible in some extreme environments, one natural question is whether it is possible to unveil how the bacteria interact with the environment by the measurement at the population level. Due to the specific biological question at hand, the biggest difference between our problem setup and the previous ones is the fact that our measurements are taken in the interior of the domain, but are macroscopic. The kind of data preparation is intrusive in the sense that photos are taken over the entire cultural dish but not only on the boundary (domain surface), so it enriches the available dataset. While optical tomography equipment can read off the velocity information, the photos usually only provide density information, except for very special cases Jeckel et al. [2019], Zhang et al. [2010] that have very high requirements on the lab equipments. Since the measurement is macroscopic, this reduces the richness of data.

In Hellmuth et al. [2022] the authors examined the theoretical aspect of this reconstruction problem with macroscopic interior data. It was shown that trading off the microscopic information for the interior data still gives us sufficient information to recover the transition kernel, but the experiments need to be accordingly designed. However, in the theoretical paper we assumed that the transition kernel is an unknown function, and thus an infinitely dimensional object, and the available data is the full map (from initial condition to density for all time and space), and thus an infinite dimensional object as well. This infinite-to-infinite setup is hard to be implemented numerically, so the theoretical results only provide a guidance but not a direct guarantee. The current paper can be seen as the numerical counterpart of Hellmuth et al. [2022]. In particular, we study, on the discrete level, if measurement data are finite in size, and the to-be-reconstructed transition kernel is also represented by a finite dimensional vector, can one still successfully recover the unknowns.

It turns out that the numerical issue is significantly more convoluted. When the dimension of K , the transition kernel, is changed from infinite to finite, we expect the amount of data needed to recover this finite-dimensional parameter should also be reduced. However, by how much and in what way is far from being clear. We will present below two different scenarios to argue that when data is prepared well, a stable reconstruction is expected, but when the data "degenerates," it loses information for a full recovery. Such well-posedness and ill-posedness are separately presented in two subsections of Section 3. Then in Section 5 we present the numerical evidence to showcase the theoretical prediction.

It should be noted that it is well within anticipation that different data preparation gives different conditioning for parameter reconstruction. This further prompts the study of experimental design. In the context of reconstructing the transition kernel in the chemotaxis equation, in Section 4 we will design a particular experimental setup that guarantees a unique reconstruction.

We should further note that reconstructing parameters for bacterial motion using the inversion perspective is not entirely new. In literature, there exist two different approaches: the first involves the utilization of statistical information at the individual level to extrapolate the microscopic transition kernel, whereas the second entails employing density data at a macroscopic scale to reconstruct certain parameters associated with a parametrized model through an optimization framework Ford and Lauffenburger [1991], Giometto et al. [2015], Salek et al. [2019], Tranquillo et al. [1988]. To our knowledge, these available studies focus on either microscopic or macroscopic models with a very limited number of unknowns to be recovered, and data of the corresponding scale are used to construct model parameters of the corresponding scale. For instance, in Pohl et al. [2017], Seyrich et al. [2018], the tumbling behavior is inferred statistically on a microscopic level, i.e. the tumbling, as an individual random process, is described by a few moments of its probability distribution that are recovered from data. In Egger et al. [2015], Fister and McCarthy [2008], the macroscopic problem was considered where parameterization emerged from discretization, and regularization was used to counter the noise. Moreover, the viewpoint of constructing the optimization problem in this article significantly differs from the existing literature. Similar as in Egger et al. [2015], Fister and McCarthy [2008], we recover the discretized version of the kinetic parameter, as this framework brings more flexibility. Our focus, however, lies on the study of well- and ill-posedness of the optimization problem related to the parameter reconstruction. To observe these effects, no regularization is applied and numerical examples are presented in a noise-free setting. This demonstrates the necessity for well-designed experimental setups, which are adapted to the fineness of the parameter discretization.

2 Framing a PDE-constrained optimization problem

We frame the problem as a PDE-constrained optimization, which is to reconstruct K that fits data as much as possible conditioned on the fact that the kinetic chemotaxis model is satisfied.

To start off, we first present the kinetic chemotaxis model. Denoting $f(t, x, v)$ the probability density distribution of bacteria in space $x \in \mathbb{R}^1$, time $t > 0$ and velocity $v \in V$, the equation writes:

$$\partial_t f + v \cdot \nabla_x f = \mathcal{K}(f) := \int_V K(x, v, v') f(x, t, v') - K(x, v', v) f(x, t, v) dv', \quad (1)$$

$$f(t = 0, x, v) = \phi(x, v) \in L^\infty_{+,c}(\mathbb{R} \times V) \quad (2)$$

where $v \cdot \nabla_x f$ characterizes the “run”-part where bacteria move straight forward with velocity v , and the terms on the right characterize the “tumble”-part, with bacteria changing from having velocity v' to v using the transitional rate $K(x, v, v') \geq 0$ and $K(x, v, v')$ is called the tumbling kernel. Initial data is given at $t = 0$ and is denoted by $\phi(x, v)$. We reduce the original problem for $(x, v) \in \mathbb{R}^3 \otimes \mathbb{S}^2$ to $(x, v) \in \mathbb{R}^1 \otimes \{\pm 1\}$ Giometto et al. [2015], Saragosti et al. [2011, 2010], i.e. the bacteria either moves to the left or to the right, and x is 1D in space. This simple setting on the one hand applies to the case when experiments are conducted in a bacteria culture tube, thus is biologically meaningful, on the other hand, it includes the difficulties of our setting of inversion. More details will be discussed in the subsequent part. Moreover, in some applications, the environment changes with time then the tumbling kernel K may depend on time as well, we focus on the time-independent case here when the outside signaling does not change.

To understand the the particle interaction with the environment, one needs to determine K and data is collected to infer it. Typically, it is unnecessary to recover it as a function, but some fine-discretization of it would suffice. To do so, we assume that K can be well represented by a list of finite many parameters:

$$K(x, v, v') = \sum_{r=1}^R K_r(v, v') \mathbf{1}_{I_r}(x), \quad (3)$$

meaning in the interval of $I_r = [a_{r-1}, a_r)$, $r = 2, \dots, R-1$ (with $a_{r-1} < a_r$ and $I_1 = (-\infty, a_1)$, $I_R = [a_{R-1}, \infty)$), $K(x, v, v')$ can be well approximated by a function independent of the spatial variable x . Since $V = \{\pm 1\}$, there are only two choices for the velocity change encrypted by $K_r(v, v')$: $K_r(1, -1)$ or $K_r(-1, 1)$, and thus there are in total $2R$ free values for K . Throughout the paper we abuse the notation and denote $K \in \mathbb{R}^{2R}$ as the unknown vector to be reconstructed. Moreover, we set:

$$K_r = [K_{r,1}, K_{r,2}], \quad \text{with} \quad K_{r,1} = K_r(1, -1) \quad K_{r,2} = K_r(-1, 1). \quad (4)$$

The dataset is also finite in size. In particular, we mathematically represent the local pixel reading of the photo by a test function $\mu_l \in L^1(\mathbb{R})$ for some l , then the data takes the form of

$$M_l(K) = \int_{\mathbb{R}} \int_V f_K(x, T, v) dv \mu_l(x) dx, \quad l = 1, \dots, L, \quad (5)$$

where f_K denotes the solution to (1) with kernel K . Denote the ground-truth transition kernel to be K_* , then the true data is:

$$y_l = M_l(K_*), \quad l = 1, \dots, L. \quad (6)$$

As discussed in Section 1, when K is reduced to be represented by a finite dimensional vector we expect the amount of data needed is also finite, but how to do the reduction for a stable reconstruction is still unknown. Mathematically, this amounts to studying the intricate relation between R and L and $\{\mu_l\}$.

The numerical inversion is presented as a PDE-constrained optimization. We aim to minimize the square loss between the simulated data $M(K)$ and the data y :

$$\begin{aligned} \min_K \quad \mathcal{C}(K) &= \min \frac{1}{2L} \sum_{l=1}^L (M_l(K) - y_l)^2 \\ \text{subject to} \quad & (1), \text{ and } (2). \end{aligned} \quad (7)$$

There are many algorithms that can be deployed to solve this minimization problem, and we are particularly interested in calling the simple gradient-descent (GD) algorithm. The update is given by:

$$K^{(n+1)} = K^{(n)} - \eta_n \nabla_K \mathcal{C}(K^{(n)}), \quad (8)$$

with a suitable step size $\eta_n \in \mathbb{R}_+$. It is a standard application of calculus-of-variation, as detailed in Appendix A, to derive that the (r, i) -th ($i = 1, 2, r = 1, \dots, R$) entry of the gradient $\nabla_K \mathcal{C}$:

$$\frac{\partial \mathcal{C}}{\partial K_{r,i}} = \int_0^T \int_{I_r} f(t, x, v'_i) (g(t, x, v'_i) - g(t, x, v_i)) dx dt, \quad (9)$$

where $(v_i, v'_i) = ((-1)^i, (-1)^{i+1})$ in analogy to notation (4) for K and g is the adjoint state that solves the adjoint equation

$$-\partial_t g - v \cdot \nabla g = \tilde{\mathcal{K}}(g) := \int_V K(x, v', v) (g(x, t, v') - g(x, t, v)) dv', \quad (10)$$

$$g(x, t = T, v) = -\frac{1}{L} \sum_{l=1}^L \mu_l(x) (M_l(K) - y_l). \quad (11)$$

Notice that by definition of the measurement procedure (5), the final condition of g in (11) is independent of v and contains the spatial test functions μ_l .

The convergence of GD in (8) is guaranteed for a suitable step size if the objective function is convex. Denoting $H_K \mathcal{C}$ the Hessian function of the loss function, we need $H_K \mathcal{C} > 0$ at least in a small neighborhood around K_* . If so, a constant step size $\eta_n = \eta = \frac{2\lambda_{\min}}{\lambda_{\max}^2}$ approximates the step size suggested in Wright and Recht [2022] for optimal convergence. Here $\lambda_{\min}, \lambda_{\max}$ denote the smallest and largest eigenvalues of $H_K \mathcal{C}(K_*)$. More sophisticated methods include line search for the step size or higher order methods for the update are also possible, see e.g. Ren [2010], Wright and Recht [2022].

To properly set up the problem, we make some general assumptions and fix some notations.

Assumption 1. We make assumptions to ensure the wellposedness of the forward problem in a feasible set, in particular:

- We will work locally in K , so we assume in a neighbourhood \mathcal{U}_{K_*} of K_* , there is a constant C_K so that for all $K \in \mathcal{U}_{K_*}$:

$$0 < \|K\|_\infty \leq C_K. \quad (12)$$

- Assume the initial data ϕ be in the space $L_{+,c}^\infty(\mathbb{R} \times V)$ of non negative, compactly supported functions with essential bound

$$\|\phi\|_{L^\infty(\mathbb{R} \times V)} =: C_\phi.$$

- Reciprocally, we assume the test functions $\mu_l, l = 1, \dots, L$, are in the space $L^1(\mathbb{R})$ with uniform L^1 bound

$$\int_{\mathbb{R}} |\mu_l| dx \leq C_\mu, \quad l = 1, \dots, L.$$

These assumptions allow us to operate f and g in the right spaces. In particular, we can give an upper bound for both the forward and adjoint solution in L_∞ sense, see Lemma B.1 and B.2 in Appendix B. In fact, these assumptions are in line with realistic modelling: the boundedness of the parameter K emerges from its interpretation as a probability of changing directions. Non-negativity and boundedness of the initial bacteria density are physical, as bacteria cannot infinitely aggregate due to volume filling effects.

3 Well-posedness vs. ill-posedness

The well-posedness of the inversion heavily depends on the data preparation. If a suitable experimental setting is arranged, the optimization problem is expected to provide local wellposedness around the groundtruth parameter K_* , so the classical GD can reconstruct the groundtruth. However, if data becomes degenerate, we also expect ill-conditioning and the GD will find it hard to converge to the global minimum. We spell out the two scenarios in the two theorems below.

Theorem 3.1. *Assume the hessian matrix of the cost function is positive definite at K_* and let the remaining assumptions of Proposition 3.1 hold, then there exists a neighbourhood U of K_* , in which the optimization problem (7) is Tykhonov well-posed. In particular, the gradient descent algorithm (8) with initial value $K_0 \in U$ converges.*

This theorem provides the well-posedness of the problem. To be specific, it spells out the sufficient condition for GD to find the global minimizer K_* . The condition of the hessian being positive definite at K_* may seem strong, but, paying attention to certain restrictions such as the minimal of measurements number $L \geq 2R$, we can carefully craft an experiment so to make sure it holds true. This line of study is in essence experimental design, as we will be more specific in Section 4.

On contrary to the previous wellposedness discussion, we also provide a negative result below on ill-conditioning.

Theorem 3.2. *Let $L = 2R$ and let Assumption 1 hold for all considered quantities. Consider a sequence $(\mu_1^{(m)})_m$ of test functions for the first measurement $M_1(K)$ for which one of the following scenarios holds:*

1. $\mu_1^{(m)} \rightarrow \mu_2$ in L^1 as $m \rightarrow \infty$.
2. $(\mu_1^{(m)})_m$ and μ_2 are mollifications of singular point-measurements in measurement points $\{(x_1^{(m)})_m, x_2\}$ such that $x_1^{(m)} \rightarrow x_2$ as $m \rightarrow \infty$. Furthermore, let the assumptions of Proposition 3.3 hold.

Then, as $m \rightarrow \infty$, the loss function cannot be strongly convex, and the convergence of the gradient descent algorithm (8) to K_ cannot be guaranteed. In scenario 2, this holds independently of the mollification parameter.*

The two theorems, to be proved in detail in Section 3.1 and 3.2 respectively, hold vast contrast to each other. The core of the difference between the two theorems is the data selection, with the former guaranteeing the convexity of the objective function, and the latter does not. To evaluate the convexity of the loss function amounts to the study of the hessian, a $2R \times 2R$ matrix:

$$H_K \mathcal{C}(K) = \frac{1}{L} \sum_{l=1}^L (\nabla_K M_l(K) \otimes \nabla_K M_l(K) + (M_l(K) - y_l) H_K M_l(K)) . \quad (13)$$

It is a well-known fact Polyak and Shcherbakov [2017] that a positive definite hessian provides the strong convexity of the loss function, and is a sufficient criterion that permits the convergence in the parameter space. If $H_K \mathcal{C}(K_*)$ is known to be positive, given in a small neighborhood, the hessian matrix does not change much, the convexity is guaranteed. Such boundedness of perturbation in the hessian is spelled out in Proposition 3.1, and Theorem 3.1 naturally follows. Theorem 3.2 is to look at the opposite side of the problem. In particular, it examines the degeneracy when two data collection points get very close. The degeneracy is reflected mathematically by the deficient rank structure in the hessian (13), prompting the collapse of the landscape of the objective function. The two scenarios of deficient ranks are presented in Proposition 3.3 and 3.2 respectively, and then Theorem 3.2 naturally follows.

3.1 Local well-posedness of the optimization problem

Generally speaking, it would not be easy to characterize the landscape of the distribution and thus hard to prescribe conditions for obtaining global convergence. However, suppose the data is prepared well enough that guarantees the positive definiteness for the Hessian $H_K \mathcal{C}(K_*)$ evaluated at the groundtruth K_* , there is a good chance that in a small neighborhood of this groundtruth, positive-definiteness persists and GD, if starts within this neighborhood, finds the global minimum to (7). This gives us a local well-posedness.

This local behavior is characterized in the following proposition.

Proposition 3.1. *Let Assumption 1 hold. Assume the Hessian $H_K \mathcal{C}(K_*)$ is positive definite at K_* , and that there is a uniform bound for the Hessian of the measurements in the neighborhood \mathcal{U}_{K_*} in the sense that $\|H_K M_l(K)(v, v')\|_F \leq C_{H_K M}$ for all $l = 1, \dots, L$ and $K \in \mathcal{U}_{K_*}$ in the Frobenius norm. Then there exists a (bounded) neighbourhood $U \subset \mathcal{U}_{K_*}$ of K_* , where $H_K \mathcal{C}(K)$ is positive definite for all $K \in U$. Moreover, the minimal eigenvalues $\lambda_{\min}(H_K \mathcal{C})$ satisfies*

$$|\lambda_{\min}(H_K \mathcal{C}(K_*)) - \lambda_{\min}(H_K \mathcal{C}(K))| \leq \|K_* - K\|_{\infty} C', \quad (14)$$

where the constant C' depends on the measurement time T , R , and the bounds C_μ , C_ϕ , C_K in Assumption 1 and $C_{H_K M}$. As a consequence, the radius of U can be chosen as $\lambda_{\min}(H_K \mathcal{C}(K_*))/C'$.

The proposition is hardly surprising. Essentially it suggests the hessian term is Lipschitz continuous with respect to its argument. This is expected if the solution to the equation is somewhat smooth. Such strategy will be spelled out in detail in the proof. With this proposition in hand, Theorem 3.1 is immediate.

Proof for Theorem 3.1. By Proposition 3.1, there exists a neighbourhood U in which the Hessian is positive definite, $H_K \mathcal{C}(K) > 0$ for all $K \in U$. Without loss of generality, we can assume that U is a convex set. By the strong convexity of \mathcal{C} in U , the minimizer $K_* \in U$ of \mathcal{C} is unique and thus the finite dimension of the parameter space $K \in \mathbb{R}^{2R}$ guarantees Tykhonov well-posed of the optimization problem (7) [Ferrentino and Boniello, 2019, Prop.3.1]. \square

Now we give the proof for Proposition 3.1. It mostly relies on the matrix perturbation theory [Horn and Johnson, 1985, Cor. 6.3.8] and continuity of the equation.

Proof for Proposition 3.1. According to the matrix perturbation theory, the minimal eigenvalue is continuous with respect to a perturbation to the matrix, we have

$$\begin{aligned} |\lambda_{\min}(H_K \mathcal{C}(K_*)) - \lambda_{\min}(H_K \mathcal{C}(K))| &\leq \|H_K \mathcal{C}(K_*) - H_K \mathcal{C}(K)\|_F \\ &\leq \frac{1}{L} \sum_l \left(\|(\nabla_K M_l \otimes \nabla_K M_l)(K_*) - (\nabla_K M_l \otimes \nabla_K M_l)(K)\|_F \right. \\ &\quad \left. + \|(M_l(K) - y_l) H_K M_l(K)\|_F \right) \\ &\leq \frac{1}{L} \sum_l \left(\|\nabla_K M_l(K_*) - \nabla_K M_l(K)\|_F (\|\nabla_K M_l(K_*)\|_F + \|\nabla_K M_l(K)\|_F) \right. \\ &\quad \left. + \|M_l(K) - y_l\| \|H_K M_l(K)\|_F \right) \end{aligned} \quad (15)$$

where we used the hessian form (13), triangle inequality and sub-multiplicativity for Frobenius norms. To obtain the bound (14) now amounts to quantifying each term on the right hand side of (15) and bounding them by $\|K_* - K\|_\infty$. This is respectively achieved in Lemmas 3.3, 3.5 and 3.6 that give controls to $M_l(K) - y_l$, $\|\nabla_K M_l(K)\|_F$ and $\|\nabla_K M_l(K_*) - \nabla_K M_l(K)\|_F$. Putting these results together, we have:

$$\begin{aligned} |\lambda_{\min}(H_K \mathcal{C}(K_*)) - \lambda_{\min}(H_K \mathcal{C}(K))| &\leq \|H_K \mathcal{C}(K_*) - H_K \mathcal{C}(K)\|_F \\ &\leq 2\|K_* - K\|_\infty C_\mu C_\phi e^{2C_K|V|T} \left[8RC_\phi C_\mu e^{2|V|C_K T} T \left(|V|T^2 + \frac{1}{C_K} \left(\frac{e^{2C_K|V|T} - 1}{2C_K|V|} - T \right) \right) \right. \\ &\quad \left. + |V|^2 T C_{H_K M} \right] \\ &=: \|K_* - K\|_\infty C'. \end{aligned}$$

The positive definiteness in a small neighborhood of K_* now follows. Finally, given $\|K_* - K\|_\infty < \lambda_{\min}(H_K \mathcal{C}(K_*))/C'$, the triangle inequality shows

$$\lambda_{\min}(H_K \mathcal{C}(K)) \geq \lambda_{\min}(H_K \mathcal{C}(K_*)) - |\lambda_{\min}(H_K \mathcal{C}(K_*)) - \lambda_{\min}(H_K \mathcal{C}(K))| > 0.$$

We note the form of C' is complicated but the dependence is spelled out in the following lemmas and summarized in the theorem statement. \square

As can be seen from the proof, Proposition 3.1 strongly relies on the boundedness of the terms in (15). We present the estimates below.

Lemma 3.3. *Let Assumptions 1 holds, then the measurement difference is upper bounded by:*

$$|M_l(K) - y_l| \leq |V|C_\mu \|(f_{K_*} - f_K)(T)\|_{L^\infty(\mathbb{R} \times V)} \leq \|K_* - K\|_\infty 2|V|^2 C_\mu C_\phi T e^{2C_K|V|T}.$$

Proof. Apply Lemma B.1 to the difference equation for $\bar{f} := f_{K_*} - f_K$

$$\partial_t \bar{f} + v \cdot \nabla_x \bar{f} = \mathcal{K}_K(\bar{f}) + \mathcal{K}_{(K_* - K)}(f_{K_*}) \quad (16)$$

with initial condition 0 and source $h = \mathcal{K}_{(K_* - K)}(f_{K_*}) \in L^1((0, T); L^\infty(\mathbb{R} \times V))$ by the regularity (39) of f_{K_*} . This leads to

$$\begin{aligned} \operatorname{ess\,sup}_{v,x} |\bar{f}|(x, t, v) &\leq \int_0^t e^{2|V|C_K(t-s)} \operatorname{ess\,sup}_{v,x} |\mathcal{K}_{(K_* - K)}(f_{K_*})(s)| \, ds \\ &\leq 2|V| \|K_* - K\|_\infty e^{2|V|C_K t} C_\phi t, \end{aligned} \quad (17)$$

where we used the estimate $\|f_{K_*}(s)\|_{L^\infty(\mathbb{R} \times V)} \leq e^{2|V|C_K s} \|\phi\|_{L^\infty(\mathbb{R} \times V)}$ from Lemma B.1 in the last step. \square

To estimate the gradient $\nabla_K M_l(K)$ and its difference, we first recall the form in (9) with \mathcal{C} changed to M_l here. Analogously, we can use the adjoint equation to explicitly represent the gradient:

Lemma 3.4. *Let Assumption 1 hold. Denote by f_K the mild solution of (1) and by $g_l \in C^0([0, T]; L^\infty(V; L^1(\mathbb{R})))$ the mild solution of*

$$\begin{aligned} -\partial_t g_l - v \cdot \nabla g_l &= \tilde{\mathcal{K}}(g_l) := \int_V K(x, v', v) (g_l(x, t, v') - g_l(x, t, v)) \, dv', \\ g_l(t = T, x, v) &= -\mu_l(x). \end{aligned} \quad (18)$$

Then

$$\frac{\partial M_l(K)}{\partial K_{r,i}} = \int_0^T \int_{I_r} f'(g'_l - g_l) \, dx \, dt, \quad (19)$$

where we used the abbreviated notation $h := h(t, x, v_i)$ and $h' := h(t, x, v'_i)$ for $h = f, g_l$, with (v_i, v'_i) defined as in (9).

We omit explicitly writing down the x, t dependence when it is not controversial. The proof for this lemma is the application of calculus-of-variation and will be omitted from here. We are now in the position to derive the estimates of the gradient norms.

Lemma 3.5. *Under Assumption 1, the gradient is uniformly bounded*

$$\|\nabla_K M_l(K)\|_F \leq \sqrt{2R} 2C_\phi C_\mu e^{2C_K|V|T} T, \quad \text{for all } K \in \mathcal{U}_K.$$

Proof. The Frobenius norm is bounded by the entries $\|\nabla M_l(K)\|_F \leq \sqrt{2R} \max_{r,i} \left| \frac{\partial M_l(K)}{\partial K_{r,i}} \right|$. Representation (19) together with (40) then gives the bound

$$\left| \frac{\partial M_l}{\partial K_{r,i}} \right| \leq 2C_\phi \int_0^T e^{2|V|C_K t} \max_v \left(\int_{\mathbb{R}} |g_l| \, dx \right) dt, \quad (20)$$

Application of lemma B.2 to $g = g_l, h = 0$ and $\psi = -\mu_l$ yields

$$\max_v \int_{\mathbb{R}} |g_l| \, dx(t) \leq \int_{\mathbb{R}} |-\mu_l(x)| \, dx e^{2C_K|V|(T-t)} \leq C_\mu e^{2C_K|V|(T-t)}, \quad (21)$$

which, when plugged into (20), gives

$$\left| \frac{\partial M_l}{\partial K_{r,i}} \right| \leq 2C_\phi C_\mu e^{2C_K|V|T} T.$$

\square

Lemma 3.6. *In the setting of Theorem 3.1 and under Assumption 1, the gradient difference is uniformly bounded in $K \in \mathcal{U}_K$ by*

$$\begin{aligned} &\|\nabla M_l(K_*) - \nabla M_l(K)\|_F \\ &\leq \sqrt{2R} \|K_* - K\|_\infty 2C_\phi C_\mu e^{2C_K|V|T} \left(|V|T^2 + \frac{1}{C_K} \left(\frac{e^{2C_K|V|T} - 1}{2C_K|V|} - T \right) \right). \end{aligned}$$

Proof. Now consider the entries of $\nabla M_l(K_\star) - \nabla M_l(K)$ to show smallness of $\|\nabla M_l(K_\star) - \nabla M_l(K)\|_F$. Rewrite, using lemma 3.4 and (40)

$$\begin{aligned} \left| \frac{\partial M_l(K_\star)}{\partial K_{r,i}} - \frac{\partial M_l(K)}{\partial K_{r,i}} \right| &= \left| \int_0^T \int_{I_r} f_{K_\star}(g'_{l,K_\star} - g_{l,K_\star}) - f_K(g'_{l,K} - g_{l,K}) \, dx \, dt \right| \\ &\leq \int_0^T \|(f_{K_\star} - f_K)(t)\|_{L^\infty(\mathbb{R} \times V)} 2 \max_v \int_{\mathbb{R}} |g_{l,K_\star}(t)| \, dx \, dt \\ &\quad + 2C_\phi \int_0^T e^{2|V|C_K t} \max_v \int_{\mathbb{R}} |(g_{l,K_\star} - g_{l,K})(t)| \, dx \, dt. \end{aligned}$$

The first summand can be bounded by (17) and (21). To estimate the second summand, apply Lemma B.2 to $\bar{g} := g_{l,K_\star} - g_{l,K}$ with evolution equation

$$\begin{aligned} -\partial_t \bar{g} - v \cdot \nabla_x \bar{g} &= \tilde{\mathcal{K}}_{K_\star}(\bar{g}) + \tilde{\mathcal{K}}_{(K_\star - K)}(g_{l,K}), \\ \bar{g}(t = T) &= 0, \end{aligned}$$

and $h = \tilde{\mathcal{K}}_{(K_\star - K)}(g_{l,K}) \in L^1((0, T); L^\infty(V; L^1(\mathbb{R})))$ by the regularity (44) of $g_{l,K} \in C^0((0, T); L^\infty(V; L^1(\mathbb{R})))$. This leads to

$$\begin{aligned} \max_v \int_{\mathbb{R}} |\bar{g}| \, dx &\leq e^{2|V|C_K(T-t)} \int_0^{T-t} \max_v \|\tilde{\mathcal{K}}_{(K_\star - K)}(g_{l,K})(T-s, v)\|_{L^1(\mathbb{R})} \, ds \\ &\leq 2|V| \|K_\star - K\|_\infty e^{2|V|C_K(T-t)} \int_0^{T-t} \max_v \|g_{l,K}(T-s, v)\|_{L^1(\mathbb{R})} \, ds \\ &\leq \|K_\star - K\|_\infty \frac{C_\mu}{C_K} e^{2|V|C_K(T-t)} (e^{2C_K|V|(T-t)} - 1), \end{aligned}$$

where we used (21) in the last line. In summary, one obtains

$$\begin{aligned} \left| \frac{\partial M_l(K_\star)}{\partial K_{r,i}} - \frac{\partial M_l(K)}{\partial K_{r,i}} \right| &\leq \|K_\star - K\|_\infty \left[\int_0^T 2|V|C_\phi t e^{2C_K|V|t} \cdot 2C_\mu e^{2C_K|V|(T-t)} \, dt \right. \\ &\quad \left. + 2C_\phi \int_0^T e^{2|V|C_K t} \frac{C_\mu}{C_K} e^{2C_K|V|(T-t)} (e^{2C_K|V|(T-t)} - 1) \, dt \right] \\ &\leq \|K_\star - K\|_\infty 2C_\phi C_\mu e^{2C_K|V|T} \left(|V|T^2 + \frac{1}{C_K} \left(\frac{e^{2C_K|V|T} - 1}{2C_K|V|} - T \right) \right). \end{aligned}$$

□

Together with the boundedness of the gradient (20), this shows that the first summands in (15) are Lipschitz continuous in K around K_\star which concludes the proof of Proposition 3.1.

3.2 Ill-conditioning for close measurements

While the positive hessian at K_\star guarantees local convergence, such positive-definiteness will disappear when data are not prepared well. Especially, when a minimal number of measurements is considered and two measurements, $M_1(K)$ and $M_2(K)$ for example, become close, we will show that the hessian degenerates, and the strongly convexity is lost, and hence the convergence to K_\star is no longer guaranteed.

The closeness of two measurements can be quantified through different manners. For example, we can argue that the two measurements are close when the two test functions μ_1, μ_2 are close in L^1 sense. Or they can be close if the reading of the measurements are taken at two locations closeby. In this case, μ_1 and μ_2 can be taken as mollifiers from direct Dirac- δ readings of the density at x_1 and x_2 , and the closeness is quantified by $|x_1 - x_2|$.

We will study how the hessian degenerates in these two scenarios. In both cases, we examine the two parts in (13) and evaluate their change as two measurements get close. In particular, the application of Lemma 3.3 already suggests the second part in (13) is negligible for K is close to K_\star and the rank structure of the hessian is predominantly controlled by the first part, which reads as the summation of many rank 1 matrices $\nabla_K M_l(K) \otimes \nabla_K M_l(K)$. When

two measurements (μ_1 and μ_2) get close, we will argue that $\nabla_K M_1(K)$ is almost parallel to $\nabla_K M_2(K)$, making the hessian lacking at least one rank, and the strong convexity is lost. Mathematically, this means we need to show $\|\nabla_K M_1(K) - \nabla_K M_2(K)\|_2 \approx 0$ when $\mu_1 \approx \mu_2$ in the two senses spelled out above.

Recalling (19), we have for every $r \in \{1, \dots, R\}$ and $i \in \{1, 2\}$

$$\begin{aligned} \frac{\partial M_1(K)}{\partial K_{r,i}} - \frac{\partial M_2(K)}{\partial K_{r,i}} &= \int_0^T \int_{I_r} f'((g_1 - g_2)' - (g_1 - g_2)) \, dx \, dt \\ &= \int_0^T \int_{I_r} f'(\bar{g}' - \bar{g}) \, dx \, dt, \end{aligned} \quad (22)$$

where $\bar{g} := g_1 - g_2$ solves (10) with final condition $\bar{g}(t = T, x, v) = \mu_2(x) - \mu_1(x)$. So the bulk of the analysis in the two subsections below is to quantify the smallness of (22) in terms of the smallness of $\mu_1(x) - \mu_2(x)$.

3.2.1 L^1 measurement closeness

The following proposition states the loss of strong convexity as $\mu_2 - \mu_1 \rightarrow 0$ in $L^1(\mathbb{R})$. In particular, the requirement of Proposition 3.1 that $H_K \mathcal{C}(K_*)$ is positive definite is no longer satisfied, so local well-posedness of the optimization problem and thus the convergence of the algorithm can no longer be guaranteed.

Proposition 3.2. *Let Assumption 1 hold. Then, as $\mu_1^{(m)} \xrightarrow{m \rightarrow \infty} \mu_2$ in $L^1(\mathbb{R})$, one eigenvalue of the Hessian $H_K \mathcal{C}(K_*)$ vanishes.*

This proposition immediately allows us to prove scenario 1 in Theorem 3.2:

Proof of Theorem 3.2. Propositions 3.2 establishes one eigenvalue of $H_K \mathcal{C}(K_*)$ vanishes as $m \rightarrow \infty$. This lack of positive definiteness and thus strong convexity of \mathcal{C} around K_* means that it cannot be guaranteed that the minimizing sequences of \mathcal{C} converge to K_* . \square

We now give the proof of the proposition.

Proof. As argued above, we show $\|\nabla_K M_1^{(m)}(K) - \nabla_K M_2(K)\|_2 \rightarrow 0$ as $m \rightarrow \infty$. Recall (22), we need to show:

$$\frac{\partial M_1^{(m)}(K)}{\partial K_{r,i}} - \frac{\partial M_2(K)}{\partial K_{r,i}} \xrightarrow{m \rightarrow \infty} 0 \quad \forall (r, i) \in \{1, \dots, R\} \times \{1, 2\}. \quad (23)$$

where $\bar{g} := g_1 - g_2$ solves (10) with final condition $\bar{g}(t = T, x, v) = \mu_2(x) - \mu_1^{(m)}(x)$. Application of Lemma B.2 gives

$$\|\bar{g}(t)\|_{L^\infty(V; L^1(\mathbb{R}))} \leq e^{2C_K|V|(T-t)} \|\mu_2 - \mu_1^{(m)}\|_{L^\infty(V; L^1(\mathbb{R}))} = e^{2C_K|V|(T-t)} \|\mu_2 - \mu_1^{(m)}\|_{L^1(\mathbb{R})}.$$

Plug this into (22) and estimate f by (40) to obtain

$$\begin{aligned} \left| \frac{\partial (M_1^{(m)} - M_2)(K)}{\partial K_{r,i}} \right| &\leq 2C_\phi \int_0^T e^{2C_K|V|t} \|\bar{g}(t)\|_{L^\infty(V; L^1(\mathbb{R}))} \, dt \\ &\leq 2C_\phi e^{2C_K|V|T} T \|\mu_2 - \mu_1^{(m)}\|_{L^1(\mathbb{R})}. \end{aligned}$$

Since every entry (r, i) converges, the gradient difference vanishes $\|\nabla_K M_1^{(m)}(K) - \nabla_K M_2(K)\|_2 \rightarrow 0$ as $m \rightarrow \infty$.

We utilize this fact to show the degeneracy of the Hessian. Noting:

$$H_K \mathcal{C}(K_*) = \underbrace{\left[\sum_{l=3}^{2R} \nabla M_l \otimes \nabla M_l + 2 \nabla M_2 \otimes \nabla M_2 \right]}_A + \underbrace{\left[\nabla M_1^{(m)} \otimes \nabla M_1^{(m)} - \nabla M_2 \otimes \nabla M_2 \right]}_{B^{(m)}}.$$

It is straightforward that the rank of A is at most $2R - 1$, so the j -th largest eigenvalue $\lambda_j(A) = 0$ vanishes for some j . Moreover, since $\|\nabla_K M_1^{(m)}(K) - \nabla_K M_2(K)\|_2 \rightarrow 0$, we have $\|B^{(m)}\|_F \rightarrow 0$. Using the continuity of the minimal eigenvalue with respect to a perturbation of the matrix, the j -th largest eigenvalue of $H_K \mathcal{C}(K_*)$ vanishes

$$|\lambda_j(H_K \mathcal{C}(K_*))| = |\lambda_j(H_K \mathcal{C}(K_*)) - \lambda_j(A)| \leq \|B^{(m)}\|_F \rightarrow 0, \quad \text{as } m \rightarrow \infty.$$

\square

3.2.2 Pointwise measurement closeness

We now study the second scenario of Theorem 3.2 and consider μ_1, μ_2 as mollifications of a singular pointwise testing. For this purpose, let $\xi \in C_c^\infty(\mathbb{R})$ be a smooth function, compactly supported in the unit ball $B_1(0)$ with $0 \leq \xi \leq 1$ and $\xi(0) = 1$. In the following, we consider the measurement test functions

$$\mu_i^\eta(x) = \frac{1}{\eta} \xi\left(\frac{x - x_i}{\eta}\right), \quad i = 1, 2. \quad (24)$$

Our aim is to show that the assertion of Theorem 3.2 is true independently of the mollification parameter $\eta > 0$. This shows that in the limit as $\eta \rightarrow 0$, i.e. in the pointwise measurement case, we still lose strong convexity around K_* .

Proposition 3.3. *Let μ_1^η, μ_2^η be of the form (24) with measurement locations $x_2 \notin \{a_r\}_{r=1, \dots, R}$ for the partition of \mathbb{R} from (3). Consider a small neighbourhood of K_* and let Assumption 1 hold. Additionally, let the measurement time T and locations be chosen such that*

$$(e^{T|V|C_K} - 1) < 1, \quad \min_r |x_2 - a_r| - T > \eta_0 > 0.$$

If the initial condition ϕ is uniformly continuous in x , uniformly in v , then $\nabla_K M_1(K) \rightarrow \nabla_K M_2(K)$ as $x_1 \rightarrow x_2$ in the standard Euclidean norm, and the convergence is independent of $\eta \leq \eta_0$.

This proposition explains the breakdown of well-posedness presented in Theorem 3.2 in the second scenario. Since the proof for the theorem is rather similar to that of the first scenario, we omit it from here.

Similar to the previous scenario, we need to show smallness of the gradient difference (22). This time, we have to distinguish two sources of smallness: For singular parts of the adjoint \bar{g} , the smallness of the corresponding gradient difference is generated by testing it on a sufficiently regular f at close measuring locations. So it is small in the weak sense. The regular parts $\bar{g}_{>N}$ of \bar{g} represent the difference of \bar{g} and its singular parts and evolve from the integral operator on the right hand side of (10), which exhibits a diffusive effect. Smallness is obtained by adjusting the cut off regularity N .

Let us mention, however, that the time constraint is mostly induced for a technical reason. In order to bound the size of the regular parts of the adjoint solution, we use the plain Grönwall inequality which leads to an exponential growth that we counterbalance by a small measuring time T . The spatial requirement $\min_r |x_2 - a_r| - T > \eta_0 > 0$ is a reflection of the fact that we need the measuring blob (support of μ) to be somewhat centered in the constant pieces of the piecewise-constant function K . This helps to force the measuring to precisely pick up only the information from that particular piece. This specific design will later be discussed in Section 4 as well.

To put the above considerations into a mathematical framework, we deploy the singular decomposition approach, and we are to decompose

$$\bar{g} = \sum_{n=0}^N \bar{g}_n + \bar{g}_{>N}, \quad (25)$$

where the regularity of \bar{g}_n increases with n . Here, we define \bar{g}_0 as the solution to

$$\begin{aligned} -\partial_t \bar{g}_0 - v \cdot \nabla_x \bar{g}_0 &= -\sigma \bar{g}_0, \\ \bar{g}_0(t = T, x, v) &= \mu_2^\eta(x) - \mu_1^\eta(x), \end{aligned}$$

for $\sigma(x, v) := \int_V K(x, v', v) dv'$, and \bar{g}_n are inductively defined by

$$\begin{aligned} -\partial_t \bar{g}_n - v \cdot \nabla_x \bar{g}_n &= -\sigma \bar{g}_n + \tilde{\mathcal{L}}(\bar{g}_{n-1}), \\ \bar{g}_n(t = T, x, v) &= 0, \end{aligned} \quad (26)$$

where we used the notation $\tilde{\mathcal{L}}(\bar{g}) := \int K(x, v', v) \bar{g}(x, t, v') dv'$. The remainder $\bar{g}_{>N}$ satisfies

$$\begin{aligned} -\partial_t \bar{g}_{>N} - v \cdot \nabla_x \bar{g}_{>N} &= -\sigma \bar{g}_{>N} + \tilde{\mathcal{L}}(\bar{g}_N + \bar{g}_{>N}), \\ \bar{g}_{>N}(t = T, x, v) &= 0. \end{aligned} \quad (27)$$

It is a straightforward calculation that

$$(22) = \sum_{n=0}^N \int_0^T \int_{I_r} f'(\bar{g}'_n - \bar{g}_n) dx dt + \int_0^T \int_{I_r} f'(\bar{g}'_{>N} - \bar{g}_{>N}) dx dt. \quad (28)$$

We are to show, in the two lemmas below, that both terms are small when $x_1 \rightarrow x_2$. To be more specific:

Lemma 3.7. *Let the assumptions of Proposition 3.3 be satisfied. For any $\varepsilon > 0$, and any $n \in \mathbb{N}_0$, there exists a $\delta_n(\varepsilon) > 0$ such that*

$$\left| \int_0^T \int_{I_r} f' \bar{g}_n dx dt \right| \leq \varepsilon, \quad \text{if } |x_1 - x_2| < \delta_n(\varepsilon). \quad (29)$$

The remainder can be bounded similarly.

Lemma 3.8. *Under the assumptions of Proposition 3.3, one has*

$$\left| \int_0^T \int_{I_r} f' \bar{g}_{>N} dx dt \right| \leq T^2 |V| C_K C_\phi e^{2|V|C_K T} (e^{C_K|V|T} - 1)^N C_\mu,$$

which becomes arbitrarily small for large N .

The proofs for both lemmas exploit the continuity of f by choice of ϕ , and the smallness of the higher regularity components of the g term. Since it is not keen to the core of the paper, we leave the details to Appendix C. The application of the two lemmas gives Proposition 3.3:

Proof of Proposition 3.3. Let $\varepsilon > 0$. Because $e^{C_K|V|T} - 1 < 1$ by assumption, we can choose $N \in \mathbb{N}$ large enough such that $2T^2|V|C_K C_\phi e^{2|V|C_K T} (e^{C_K|V|T} - 1)^N < \frac{\varepsilon}{2}$. Furthermore, let $|x_1 - x_2| < \min_{n \leq N} \delta_n(\frac{\varepsilon}{4(N+1)})$. Then with the triangle inequality and Lemmas 3.7 and 3.8, we obtain from (28)

$$\begin{aligned} \left| \frac{\partial(M_1 - M_2)(K)}{\partial K_{r,i}} \right| &\leq \sum_{n=0}^N \left| \int_0^T \int_{I_r} f'(\bar{g}'_n - \bar{g}_n) dx dt \right| + \left| \int_0^T \int_{I_r} f'(\bar{g}'_{>N} - \bar{g}_{>N}) dx dt \right| \\ &\leq 2N \frac{\varepsilon}{4(N+1)} + 2T^2|V|C_K C_\phi e^{2|V|C_K T} (e^{C_K|V|T} - 1)^N C_\mu \\ &\leq \varepsilon. \end{aligned}$$

□

4 Experimental Design

As discussed in the previous sections, it is clear that different setups bring different conditioning to the inverse problem. We are to study a particular design where the well-posedness can be ensured. To be more specific, in Proposition 3.1 we require the positive-definiteness of the Hessian term at K_* . This is a strong assumption and is typically not true unless certain initial condition and the measuring setups are in place. We propose to use the following:

Design (D). *We divide the domain $I = [a_0, a_R]$ into R intervals $I = \bigcup_{r=1}^R I_r$ with $I_r = [a_{r-1}, a_r]$, and the center for each interval is denoted by $a_{r-1/2} := \frac{a_{r-1} + a_r}{2}$. The spatial supports of the values $K_r(v, v')$ takes on the form of (3). The design is:*

- initial condition $\phi(x, v) = \sum_{r=1}^R \phi_r(x)$ is a sum of R positive functions ϕ_r that are compactly supported in $a_{r-1/2} + [-d, d]$ with $d < \min\left(\frac{a_r - a_{r-1}}{4}\right)$, symmetric and monotonously decreasing in $|x - a_{r-1/2}|$ (for instance, a centered Gaussian with a cut-off tail);
- measurement test functions $\mu_{l_i} = \bar{C}_\mu \mathbb{1}_{[(-1)^i T - d_\mu, (-1)^i T + d_\mu] + a_{r-1/2}}$, $i = 1, 2$, for some $\bar{C}_\mu > 0$, centered around $a_{r-1/2} \pm T$ with $d_\mu \leq d$;
- measurement time T such that

$$T < \min \left((1 - \delta) \frac{0.09}{C_K |V|}, \min_r \left(\frac{a_r - a_{r-1}}{4} - \frac{d}{2} \right) \right) \quad (30)$$

$$\text{for } \delta = (d + d_\mu)/T < e^{-TC_K|V|}. \quad (31)$$

Remark 4.1. Note that this design requires a delicate balancing between T and d and d_μ . Requirement (30) prescribes that T must not be too large. On the other hand, (31) requires that it must not be too small compared to d, d_μ . An exemplary choice of $d = d_\mu = cT^2$ for some $c > 0$, for instance, automatically verifies requirement (31) for small enough T .

This particular design of initial data and measurement is to respond to the fact that the equation has a characteristic and particles moves along the trajectories. The measurement is set up to single out the information we would like to reconstruct along the propagation. The visualization of this design is plotted in Figure 1.

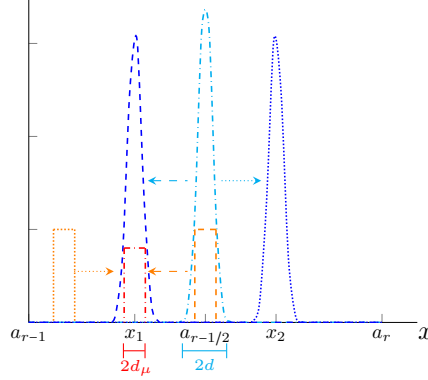


Figure 1: Motion of the ballistic parts $f^{(0)}(t=0, v)$ (cyan, dashdotted) to $f^{(0)}(t=T, v=+1)$ (blue, dotted) and $f^{(0)}(t=T, v=-1)$ (blue, dashed) and $g_1^{(0)}(t=0, v=+1)$ (orange, dotted) and $g_1^{(0)}(t=0, v=-1)$ (orange, dashed) to $g_1^{(0)}(t=T, v)$ (red, dashdotted), compare also (34).

Under this design, we have the following proposition:

Proposition 4.1. *The design (D) decouples the reconstruction of K_r . To be more specific, recall (4)*

$$K = [K_r], \quad \text{with} \quad K_r = [K_{r,1}, K_{r,2}].$$

The Hessian $H_K C$ has a block diagonal structure with each of the blocks is a 2×2 matrix given by the Hessian $H_{K_r} C$.

Proof. By the linearity of (1), (10), their solutions $f = \sum_{r=1}^R f_r$ and $g = \sum_{r=1}^R \sum_{i=1}^2 g_{l_i^r}$ decompose into solutions f_r of (1) with initial conditions ϕ_r and $g_{l_i^r}$ with final condition $-(M_{l_i^r} - y_{l_i^r})\mu_{l_i^r}/2R$, the summands of the final condition (11), correspondingly. By construction of T and the constant speed of propagation $|v| = 1$, the spatial supports of f_r and $g_{l_1^r}, g_{l_2^r}$ are fully contained only in I_r for all $t \in [0, T], v \in V$. As such, only f_r and $g_{l_j^r}$ carry information about K_r , and no information for other K_s with $s \neq r$. \square

This not only makes boundary conditions superfluous, but also translates the problem of finding a $2R$ valued vector K into R individual smaller problems of finding the two-constant pair $(K_{r,1}, K_{r,2})$ within I_r . This comes with the cost of prescribing very detailed measurements depending on the experimental scales I_r and d , but opens the door for parallelized computation.

Furthermore, under mild conditions, this design ensures the local reconstructability of the inverse problem.

Theorem 4.2. *Let Assumption 1 hold. Given the Hessian $H_K M_1(K)$ is bounded in Frobenius norm in a neighbourhood of K_* , Design (D) generates a locally well-posed optimization problem (7).*

The proof is layed out in the subsequent subsection 4.1.

Remark 4.3. Let us mention that the bounds for T in Design (D) are not optimal. In the proof of theorem 4.2 we used crude estimates, and we believe these estimates can potentially be relaxed to allow for longer measurement times T . Furthermore, the setup can easily be modified to use different measurement times for different intervals I_r , for instance. In this case, again, the bounds on T can be relaxed.

Remark 4.4. Design (D) shares similarities with the theoretical reconstruction setting in Hellmuth et al. [2022], where a pointwise reconstruction of a continuous kernel \tilde{K} was obtained by a sequence of experiments where the measurement time T became small and the measurement location gets close to the initial location. The situation is also seen here. As we refine the discretization for the underlying K -function using higher dimensional vector, measurement time has to be shortened to honor the refined discretization. However, we should also note the difference. In Hellmuth et al. [2022], we studied the problem in higher dimension and thus explicitly excluded the ballistic part of the data from the measurement

4.1 Proof of Theorem 4.2

Given Theorem 3.1, it remains to prove $H_K \mathcal{C}(K_*) > 0$. As the Hessian attains a block diagonal structure (Proposition 4.1), we are to study the 2×2 -blocks

$$H_{K_r} \mathcal{C}(K_*) = \nabla_{K_r} M_{l_1^r}(K_*) \otimes \nabla_{K_r} M_{l_1^r}(K_*) + \nabla_{K_r} M_{l_2^r}(K_*) \otimes \nabla_{K_r} M_{l_2^r}(K_*). \quad (32)$$

Here the two measurements $M_{l_1^r}, M_{l_2^r}$ are inside I_r , and $\nabla_{K_r} = [\partial_{K_{r,1}}, \partial_{K_{r,2}}]$. The positive definiteness of the full $H_K \mathcal{C}(K_*)$ is equivalent to the positive definiteness of each individual $H_{K_r} \mathcal{C}(K_*)$. This is established in the subsequent proposition.

Proposition 4.2. *Let Assumption 1 hold. If the Hessian $H_K M_l(K)$ is bounded in Frobenius norm in a neighbourhood of K_* , then the Design (D) produces a positive-definite hessian $H_K \mathcal{C}(K_*)$.*

According to (32), $H_{K_1} \mathcal{C}(K_*)$ is positive definite if

$$\left| \frac{\partial M_1(K_*)}{\partial K_{1,1}} \right| > \left| \frac{\partial M_1(K_*)}{\partial K_{1,2}} \right| \quad \text{and} \quad \left| \frac{\partial M_2(K_*)}{\partial K_{1,1}} \right| < \left| \frac{\partial M_2(K_*)}{\partial K_{1,2}} \right| \quad (33)$$

holds true for the measurements M_1, M_2 corresponding to K_1 . Due to design symmetry, it is sufficient to study the first inequality. Consider the difference $\frac{\partial M_1(K_*)}{\partial K_{1,1}} - \frac{\partial M_1(K_*)}{\partial K_{1,2}}$. Similar to (25) and (28), we are to decompose the equation for f and g ((1) and (18) respectively, with $K = K_*$) into the ballistic parts $g_1^{(0)}$ and $f^{(0)}$ and the remainder terms. Namely, let $g_1^{(0)}$ and $f^{(0)}$ satisfy

$$\begin{cases} -\partial_t g_1^{(0)} - v \cdot \nabla_x g_1^{(0)} &= -\sigma g_1^{(0)} \\ g_1^{(0)}(t = T, x, v) &= \mu_1(x) \end{cases} \quad \text{and} \quad \begin{cases} \partial_t f^{(0)} - v \cdot \nabla_x f^{(0)} &= -\sigma f^{(0)} \\ f^{(0)}(t = 0, x, v) &= \phi(x, v). \end{cases} \quad (34)$$

Then the following two lemmas are in place with $\mu_1(x)$ and $\phi(x, v)$ as in Design (D).

Lemma 4.5. *In the setting of Proposition 4.2, for $(v, v') = (+1, -1)$, the ballistic part*

$$B := \left| \int_0^T \int_{I_1} f^{(0)}(v') (g_1^{(0)}(v') - g_1^{(0)}(v)) dx dt \right| - \left| \int_0^T \int_{I_1} f^{(0)}(v) (g_1^{(0)}(v) - g_1^{(0)}(v')) dx dt \right| \quad (35)$$

satisfies

$$B \geq C_{\phi\mu} (e^{-TC_K|V|T} - (d_\mu + d)) > 0, \quad (36)$$

where $C_{\phi\mu} = \int_{I_1} \phi_1(x) \mu_1(-T + x) dx = \max_{a,b} \int_{I_1} \phi_1(x + a) \mu_1(-T + x + b) dx$ by construction of ϕ_1, μ_1 .

At the same time, the remainder term is small.

Lemma 4.6. *In the setting of Proposition 4.2, the remaining scattering term*

$$S := \int_0^T \int_{I_1} f(v') (g_1(v') - g_1(v)) dx dt - \int_0^T \int_{I_1} f^{(0)}(v') (g_1^{(0)}(v') - g_1^{(0)}(v)) dx dt$$

is bounded uniformly in (v, v') by

$$|S| \leq 4C_{\phi\mu} T \frac{C_K |V| T}{(1 - C_K |V| T)^2}. \quad (37)$$

Proposition 4.2 is a corollary of Lemmas 4.5, 4.6.

Proof of Proposition 4.2. By the bounds obtained in lemmas 4.5, 4.6, one has

$$\begin{aligned} & \left| \frac{\partial M_1(K_*)}{\partial K_{1,1}} \right| - \left| \frac{\partial M_1(K_*)}{\partial K_{1,2}} \right| \geq B - 2|S| \\ & \geq C_{\phi\mu} (e^{-TC_K|V|T} - (d_\mu + d)) - 8C_{\phi\mu} T \frac{C_K |V| T}{(1 - C_K |V| T)^2} \\ & \geq C_{\phi\mu} T \left(1 - TC_K |V| - \delta - 8 \frac{0.09(1 - \delta)}{(1 - 0.09)^2} \right). \end{aligned}$$

By assumption $0 < T < (1 - \delta) \frac{0.09}{C_K |V|}$ with $\delta = \frac{d + d_\mu}{T} < 1$, the last line is positive. In total, this shows the first part of inequality (33). As the second part can be treated in analogy, it follows that $H_{K_1} \mathcal{C}(K_*)$ is positive definite. \square

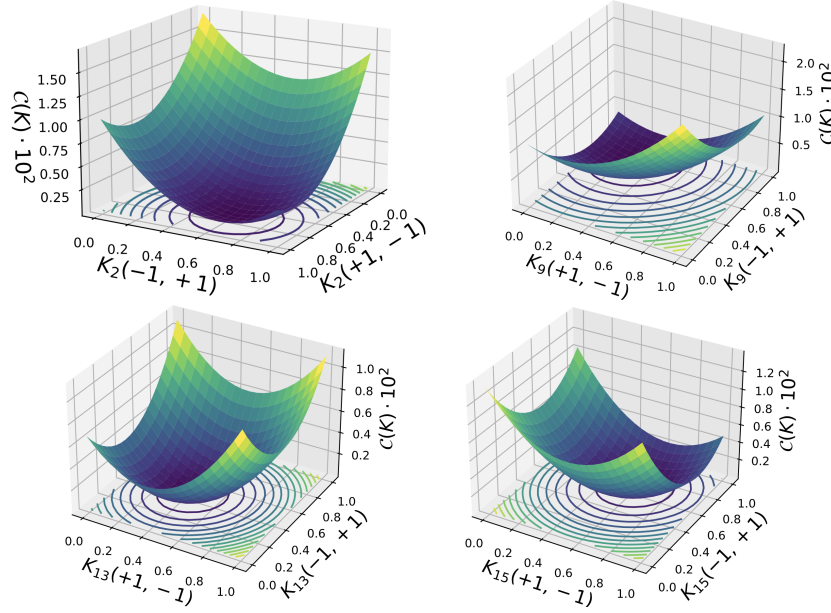


Figure 2: (Marginal) loss functions $\mathcal{C}(K)$ for $R = 20$: For a fixed $r \in \{2, 9, 13, 15\}$, we plot \mathcal{C} as a function of K_r with all $K_{s \neq r}$ set to be the groundtruth $(K_\star)_s$.

Finally, Theorem 4.2 is a direct consequence of Proposition 4.2.

Proof of Theorem 4.2. Repeated application of the arguments to all $H_{K_r} \mathcal{C}(K_\star)$, $r = 1, \dots, R$ shows that $H_K \mathcal{C}(K_\star) > 0$. Assuming boundedness of the Hessian $H_K M_l(K)$ in a neighbourhood of K_\star , theorem 3.1 proves local well-posedness of the inverse problem. \square

The proofs for the Lemmas 4.5-4.6 are rather technical and we leave them to Appendix D. Here we only briefly present the intuition. According to Figure 1, $f^{(0)}(v' = -1)$ and $g_1^{(0)}(v' = -1)$ have a fairly large overlapping support, whereas $g_1^{(0)}(v = +1)$ overlaps with $f^{(0)}(v' = -1)$ and $g_1^{(0)}(v' = -1)$ with $f^{(0)}(v = +1)$ only for a short time spans $T \approx T$ and $T \approx 0$ respectively. Recalling (35), we see the negative components of the term B are small, making B positive overall. The smallness of S is a result of small measurement time T .

5 Numerical experiments

As a proof of concept for the prediction given by the theoretical results in Section 3, we present some numerical evidence.

An explicit finite difference scheme is used for the discretization of (1) and (10). In particular, the transport operator is discretized by the Lax-Wendroff method and the operator \mathcal{K} is treated explicitly in time. The scheme is consistent and stable when $\Delta t \leq \min(\Delta x, C_K^{-1})$, and thus it converges according to the Lax-Equivalence theorem. More sophisticated solvers for the forward model Filbet and Yang [2014] can be deployed when necessary. Also, when a compatible solver Apel and Flaig [2012] for the adjoint equation exists, these pairs of solvers can readily be incorporated in the inversion setting.

All subsequent experiments were conducted with noise free synthetic data $y_l = M_l(K_\star)$ that was generated by a forward computation with the true underlying parameter K_\star .

5.1 Illustration of well-posedness

In Section 4, it was suggested a specific design of initial data and measurement mechanism can provide a successful reconstruction of the kernel K , and that the loss function is expected to be strongly convex. We observe it numerically as well. In particular, we set $R = 20$ and use Gaussian initial data, and plot the (marginal) loss function in Figure 2. Figure 3 depicts the convergence of some parameter values $K_r(v, v')$ in this scenario against the corresponding loss

function value. An exponential decay of the loss function, as expected from theory [Polyak and Shcherbakov, 2017, Th.3], can be observed.

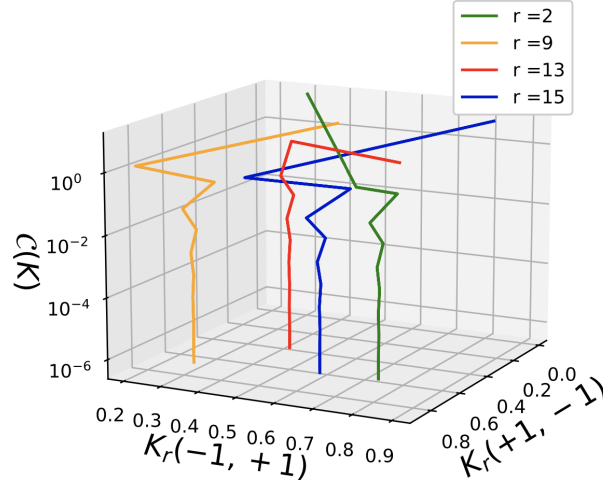


Figure 3: Convergence of the parameter values $K_r(v, v')$ from (3) for $r = 2, 9, 13, 15$ to the ground truth as the cost function converges.

The strictly positive-definiteness feature persists in a small neighborhood of the optimal solution K_* . This means adding a small perturbation to K_* , the minimal eigenvalue of the Hessian matrix $H_K \mathcal{C}(K)$ stays above zero. In Figure 4 we present, for two distinct experimental setups, the minimum eigenvalue as a function of the perturbation to $K_r(v, v')$. In both cases, the green spot (the groundtruth) is positive, and it enjoys a small neighborhood where the minimum eigenvalue is also positive, as predicted by Theorem 3.1. In the right panel, we do observe, as one moves away from the groundtruth, the minimal eigenvalue takes on a negative value, suggesting the loss of convexity. This numerically verifies that the well-posedness result in Theorem 3.1 is local in nature. The panel on the left deploys the experiment design provided by Section 4. The simulation is ran over the entire domain of $[0, 1]^2$ and the positive-definiteness stays throughout the domain, hinting the proposed experimental design (D) can potentially be globally well-posed. To generate the plots, a simplified setup with $R = 2$ and constant initial data was considered.

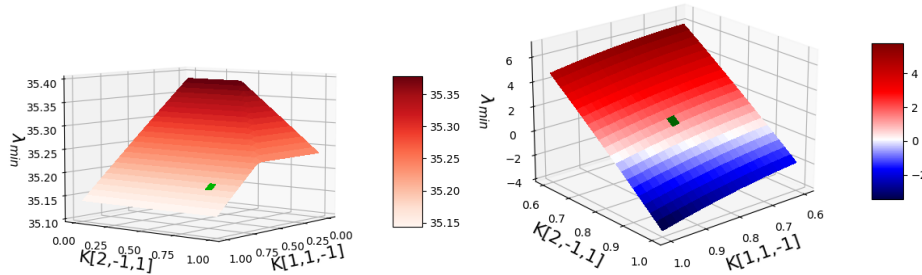


Figure 4: Minimal eigenvalues of the Hessian $H_K \mathcal{C}(K)$ around the true parameter K_* for two experimental designs. We perturb K by changing values in $K_1(1, -1)$ and $K_2(-1, 1)$. The groundtruth is marked green in both plots.

5.2 Ill-conditioning for close measurement locations

We now provide numerical evidence to reflect the assertion from 3.2. In particular, the strong convexity of the loss function would be lost if measurement location x_1 becomes close to x_2 .

We summarize the numerical evidence in Figure 5. Here we still use $R = 20$ and constant initial data but vary the detector positions. To be specific, we assign values to x_1 using $\{x_1^{(0)} = c_1 - T, x_1^{(1)} = c_1 + \frac{T}{2}, x_1^{(2)} = c_1 + \frac{4}{5}T, x_1^{(3)} = x_2 = c_1 + T\}$. As the superindex grows, $x_1 \rightarrow x_2$ with $x_1^{(3)} = x_2$ when the two measurements exactly coincide. For $x_1 = x_2$, the cost function is no longer strongly convex around the ground truth K_* , as its hessian is singular. The thus induced

vanishing learning rate $\eta = \frac{2\lambda_{\min}}{\lambda_{\max}^2}$ was exchanged by the learning rate for $x_1 = x_1^{(2)}$ in this case to observe the effect of the gradient.

In the first, third and fourth panel of Figure 5, we observe that the cost function as well as the parameter reconstructions for K_9 and K_{15} nevertheless converge, but convergence rates that slow down significantly comparing purple (for $x_1^{(0)}$), blue (for $x_1^{(1)}$), green (for $x_1^{(2)}$) and orange (for $x_1^{(3)}$) due to smaller learning rates. The overlap of the parameter reconstructions for $x_1 \in \{x_1^{(2)}, x_1^{(3)}\}$ is due to the coinciding choice of the learning rate and a very similar gradient for parameters K_9, K_{15} whose information is not reflected in the measurement in x_1 .

As parameter K_1 directly affects the measurement at x_1 , Panel 2 showcases the degenerating effect of the different choices of x_1 on the reconstruction. Whereas convergence is still obtained in the blue curve (for $x_1^{(1)}$), the reconstructions of K_1 from measurements at $x_1^{(2)}$ (green) and $x_1^{(3)}$ (orange) clearly fail to converge to the true parameter value in black. This offset seems to grow with stronger degeneracy in the measurements.

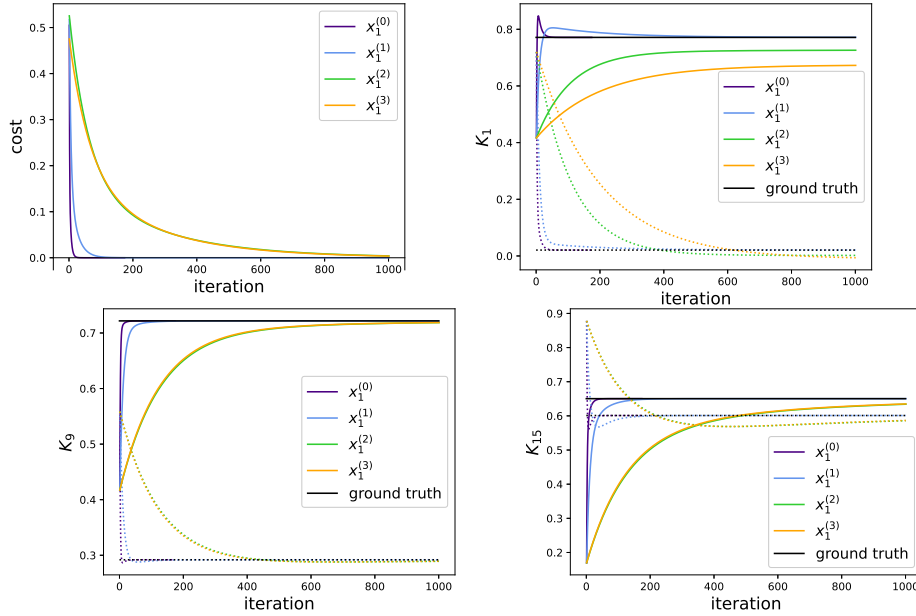


Figure 5: Cost function and reconstructions of $K_r(+1, -1)$ (solid lines) and $K_r(-1, +1)$ (dotted lines) for $r = 1, 9, 15$ and $R = 20$ under different measurement locations for x_1 . x_1 takes the values of $\{x_1^{(0)} = c_1 - T, x_1^{(1)} = c_1 + \frac{T}{2}, x_1^{(2)} = c_1 + \frac{4}{5}T, x_1^{(3)} = c_1 + T\}$ with $x_1^{(3)} = x_2$.

6 Discussion

In this paper we present an optimization framework for the reconstruction of the velocity jump parameter K in the chemotaxis equation (1) using velocity averaged measurements (5) from the interior domain. In the numerical setting when PDE-constrained optimization is deployed, depending on the experimental setup, the problem is can be either locally well-posedness or ill-conditioned. We further propose a specific experimental design that is adaptive to the discretization of K . This design decouples the reconstruction of local values of the parameter K using the corresponding measurements. The design thus opens up opportunities to parallelization. As a proof of concept, numerical evidence were presented. They are in good agreement with the theoretical predictions

A natural extension of the results presented in the current paper is the algorithmic performance in higher dimensions. The theoretical findings seem to apply in a straightforward manner, but details need to be evaluated. Numerically one can certainly also refine the solver implementation. For example, it is possible that higher order numerical PDE solvers that preserve structures bring extra benefit. More sophisticated optimization methods such as the (Quasi-)Newton method or Sequential Quadratic Programming are possible alternatives for conducting the inversion Burger and Mühlhuber [2002], Haber et al. [2000], Ren [2010], Smyl et al. [2021]. Furthermore, we adopted a first optimize, then discretize approach in this article. Suggested in Apel and Flaig [2012], Gunzburger [2002], Liu and Wang [2019], a first discretize, then

optimize framework could be bring automatic compatibility of forward and adjoint solvers, but extra difficulties Hinze et al. [2008] need to be resolved.

Our ultimate goal is to form a collaboration between practitioners to solve the real-world problem related to bacteria motion reconstruction Le [2002]. To that end, experimental design is non avoidable. A class of criteria proposed under the Bayesian shed light, see Alexanderian [2021] and references therein. In our context, it translates to whether the design proposed in Section 4 satisfies these established optimality criteria.

A Derivation of the gradient (9)

This section justifies formula (9) for the gradient of the cost function \mathcal{C} with respect to K . Let us first introduce some notation: Denote by

$$\mathcal{J}(f) := \frac{1}{2L} \sum_{l=1}^L \left(\int_{\mathbb{R}} \int_V f(T, x, v) dv \mu_l(x) dx - y_l \right)^2$$

the loss for $f \in \mathcal{Y} = \{h \mid h, \partial_t h + v \cdot \nabla h \in C^0([0, T]; L^\infty(\mathbb{R} \times V))\}$. Note that mild solutions of (1) are contained in \mathcal{Y} , since $\mathcal{K}(f) \in C^0([0, T]; L^\infty(\mathbb{R} \times V))$ by regularity of f from Lemma B.1. Then $\mathcal{C}(K) := \mathcal{J}(f_K)$ in the notation of (5). The Lagrangian function for the PDE constrained optimization problem (7) reads

$$\mathcal{L}(K, f, g, \lambda) = \mathcal{J}(f) + \langle g, \partial_t f + v \cdot \nabla f - \mathcal{K}(f) \rangle_{x,v,t} + \langle \lambda, f(t=0) - \phi \rangle_{x,v},$$

for $f \in \mathcal{Y}$ and $g \in \mathcal{Z} = \{h \mid h, \partial_t h + v \cdot \nabla h \in C^0([0, T]; L^\infty(V; L^1(\mathbb{R})))\}$. For $f = f_K$, our cost function $\mathcal{C}(K) = \mathcal{J}(f_K) = \mathcal{L}(K, f_K, g, \lambda)$ and

$$\frac{d\mathcal{C}(\hat{K})}{dK} = \frac{\partial \mathcal{L}}{\partial K} \Big|_{\substack{K=\hat{K}, \\ f=f_{\hat{K}}}} + \frac{\partial \mathcal{L}}{\partial f} \Big|_{\substack{K=\hat{K}, \\ f=f_{\hat{K}}}} \frac{\partial f_K}{\partial K} \Big|_{K=\hat{K}}$$

To avoid the calculation of $\frac{\partial f_K}{\partial K}$, choose the Lagrange multipliers g, λ such that $\frac{\partial \mathcal{L}}{\partial f} \Big|_{\substack{K=\hat{K}, \\ f=f_{\hat{K}}}} = 0$. Then

$$\begin{aligned} \frac{d\mathcal{C}(\hat{K})}{dK_r} &= \frac{\partial \mathcal{L}}{\partial K_r} \Big|_{\substack{K=\hat{K}, \\ f=f_{\hat{K}}}} = - \frac{\partial \langle g, \mathcal{K}_K(f) \rangle_{x,t,v}}{\partial K_r} \Big|_{\substack{K=\hat{K}, \\ f=f_{\hat{K}}}} \\ &= \int_0^T \int_{I_r} f_{\hat{K}}(x, t, v') (g(x, t, v') - g(x, t, v)) dx dt. \end{aligned}$$

To compute the gradient, g has to be specified. Recall the requirement

$$\begin{aligned} 0 &= \frac{\partial \mathcal{L}}{\partial f} \Big|_{\substack{K=\hat{K}, \\ f=f_{\hat{K}}}} \\ &= \frac{1}{L} \sum_{l=1}^L \left(\int_{\mathbb{R}} \int_V f(T) dv \mu_l(x) dx - y_l \right) \frac{\partial}{\partial f} \langle \mu_l, f(T) \rangle_{x,v} \Big|_{\substack{K=\hat{K}, \\ f=f_{\hat{K}}}} \\ &\quad + \frac{\partial}{\partial f} \left[\langle g, \partial_t f + v \cdot \nabla f - \mathcal{K}_K(f) \rangle_{x,t,v} + \langle \lambda, f(t=0) \rangle_{x,v} \right] \Big|_{\substack{K=\hat{K}, \\ f=f_{\hat{K}}}} \end{aligned} \tag{38}$$

We will motivate the choice of g such that the derivatives cancel out each other. Because we are dealing with mild solutions where integration by parts in time and space cannot be used right away, we approximate f and g by sequences of functions

- $(f^n)_n \subset C^1([0, T]; L^\infty(\mathbb{R} \times V)) \cap C^0([0, T]; W^{1,\infty}(\mathbb{R}; L^\infty(V)))$ that converge $f_n \rightarrow f$ with $\partial_t f_n + v \cdot \nabla f_n \rightarrow \partial_t f + v \cdot \nabla f$ in $C^0([0, T]; L^\infty(\mathbb{R} \times V))$ and
- $(g^n)_n \subset C^1([0, T]; L^\infty(V; L^1(\mathbb{R}))) \cap C^0([0, T]; L^\infty(V; W^{1,1}(\mathbb{R})))$ with $g_n \rightarrow g$ with $-\partial_t g_n - v \cdot \nabla g_n \rightarrow -\partial_t g - v \cdot \nabla g$ in $C^0([0, T]; L^\infty(V; L^1(\mathbb{R})))$.

This is possible, because the respective spaces for f_n and g_n are dense in \mathcal{Y} and \mathcal{Z} . Replacing f by f_n and g by g_n in $\langle g, \partial_t f + v \cdot \nabla f - \mathcal{K}(f) \rangle_{x,t,v}$, we obtain

$$\begin{aligned} \langle g, \partial_t f + v \cdot \nabla f - \mathcal{K}(f) \rangle_{x,t,v} &= \lim_n \langle g_n, \partial_t f_n + v \cdot \nabla f_n - \mathcal{K}(f_n) \rangle_{x,t,v} \\ &= \lim_n (\langle -\partial_t g_n - v \cdot \nabla g_n - \tilde{\mathcal{K}}(g_n), f_n \rangle_{x,t,v} + \langle f_n(t=T), g_n(t=T) \rangle_{x,v} - \langle f_n(t=0), g_n(t=0) \rangle_{x,v}) \\ &= \langle -\partial_t g - v \cdot \nabla g - \tilde{\mathcal{K}}(g), f \rangle_{x,t,v} + \langle f(t=T), g(t=T) \rangle_{x,v} - \langle f(t=0), g(t=0) \rangle_{x,v}, \end{aligned}$$

where

$$\tilde{\mathcal{K}}_K(g) := \int_V K(x, v', v) (g(x, t, v') - g(x, t, v)) dv'.$$

Now, collect all terms in (38) with the same integration domain and equate them to 0. This leads to

$$\begin{aligned} -\partial_t g - v \cdot \nabla g - \tilde{\mathcal{K}}_K(g) &= 0 & \text{in } x \in \mathbb{R}, v \in V, t \in (0, T) \\ g(x, t = T, v) &= -\frac{1}{L} \sum_{l=1}^L \left(\int_{\mathbb{R}} \int_V f(T, x, v) dv \mu_l(x) dx - y_l \right) \mu_l(x) & \text{in } x \in \mathbb{R}, (v \in V) \\ \lambda &= g(t = 0) & \text{in } x \in \mathbb{R}, v \in V. \end{aligned}$$

Note that since g reflects the measurement procedure, it makes sense that $g(t = T)$ is isotropic in v . For computation of $\frac{dC(\hat{K})}{dK_r}$, use the solution g to the first two equations with kernel $K = \hat{K}$ and $f = f_{\hat{K}}$.

B Some a-priori estimates

By Assumption 1, semigroup theory yields the existence of a mild solution to (1)–(2).

Lemma B.1. *Let Assumption 1 hold and assume $h \in L^1((0, T); L^\infty(\mathbb{R} \times V))$. Then there exists a mild solution*

$$f \in C^0([0, T]; L^\infty(\mathbb{R} \times V)) \quad (39)$$

to

$$\begin{aligned} \partial_t f + v \cdot \nabla_x f &= \mathcal{K}(f) + h, \\ f(t = 0, x, v) &= \phi(x, v) \in L^\infty_+(\mathbb{R} \times V) \end{aligned}$$

that is bounded

$$\max_v \|f(t)\|_{L^\infty(\mathbb{R})} \leq e^{2|V|C_K t} C_\phi + \int_0^t e^{2|V|C_K(t-s)} \|h(s)\|_{L^\infty(\mathbb{R} \times V)} ds.$$

We carry out the proof once to make clear, how the constant in the bound is derived.

Proof. Rewrite (1) as

$$\partial_t f = \mathcal{A}f + \mathcal{B}f + h$$

with operators $\mathcal{A} : \mathcal{D}(\mathcal{A}) \rightarrow \mathcal{X}, f \mapsto -v \cdot \nabla_x f$ and $\mathcal{B} : \mathcal{X} \rightarrow \mathcal{X}, f \mapsto \mathcal{K}(f)$, where the function spaces $\mathcal{D}(\mathcal{A}) := W^{1,\infty}(\mathbb{R}; L^\infty(V))$ and $\mathcal{X} := L^\infty(\mathbb{R} \times V)$ are used. The transport operator \mathcal{A} generates a strongly continuous semigroup $T(t)u(x) = u(x - vt)$ with operator norm $\|T(t)\| \leq 1$. Clearly, \mathcal{B} is bounded in operator norm by $2|V|C_K$. The bounded perturbation theorem, see e.g. Engel and Nagel [2001], shows that $\mathcal{A} + \mathcal{B}$ generates a strongly continuous semigroup S with $\|S(t)\| \leq e^{2|V|C_K t}$. As $\phi \in \mathcal{X}$, (1) admits a mild solution

$$f(t) = S(t)\phi + \int_0^t S(t-s)h(s) ds.$$

□

The regularity of the solution of (1)–(2) is improved by more regular initial data. This is exploited in the proof of ill-conditioning for pointwise measurement closeness in Theorem 3.2.

Corollary B.1. *Let Assumption 1 hold.*

a) *Equation (1) has a mild solution f is bounded*

$$\max_v \|f(t)\|_{L^\infty(\mathbb{R})} \leq e^{2|V|C_K t} C_\phi \leq e^{2|V|C_K T} C_\phi =: C_f. \quad (40)$$

b) *If, additionally, the initial data ϕ is uniformly continuous in x , uniformly in v , then f is uniformly continuous in x , uniformly in v, t , i.e. $\max_v |f(t, x, v) - f(t, y, v)| < \varepsilon$ for all $t \in [0, T]$, if $|x - y| < \delta(\varepsilon)$.*

Proof. Assertion a) is a direct consequence of lemma B.1. We focus on proving assertion b). Let $\varepsilon > 0$. By uniform continuity of ϕ in x , one can choose δ' such that

$$\operatorname{ess\,sup}_{|x-y|<\delta', v} |\phi(x, v) - \phi(y, v)| < e^{-2C_K|V|T} \varepsilon / 2. \quad (41)$$

Now consider $\delta := \min\left(\delta', \frac{\varepsilon e^{-2C_K|V|T}}{8C_f|V|C_K(R-1)}\right)$. Integration along characteristics yields

$$\begin{aligned}
 & \operatorname{ess\,sup}_{|x-y|<\delta, v} |f(t, x, v) - f(t, y, v)| \\
 & \leq \operatorname{ess\,sup}_{|x-y|<\delta, v} |\phi(x - vt, v) - \phi(y - vt, v)| \\
 & \quad + \operatorname{ess\,sup}_{|x-y|<\delta, v} \left| \int_0^t \mathcal{K}(f)(t-s, x-vs, v) - \mathcal{K}(f)(t-s, y-vs, v) \, ds \right| \\
 & \leq \operatorname{ess\,sup}_{|x-y|<\delta, v} |\phi(x, v) - \phi(y, v)| \\
 & \quad + 2C_K|V| \int_0^t \operatorname{ess\,sup}_{|x-y|<\delta, v'} |f(s, x, v') - f(s, y, v')| \, ds \\
 & \quad + 2C_f|V| \operatorname{ess\,sup}_{|x-y|<\delta, v} \int_0^t \max_{v', v''} |K(x-vs, v', v'') - K(y-vs, v', v'')| \, ds \\
 & =: (i) + (ii) + (iii),
 \end{aligned}$$

where $(i) \leq \frac{\varepsilon}{2} e^{-2C_K|V|T}$ by (41). By symmetry, $(iii) = 2 \cdot (iv)$ where (iv) coincides with (iii) , but $x \geq y$. As K is a step function in space (3), its difference can only be non zero if a jump occurred between $x - vs$ and $y - vs$. Boundedness of K in (12) then lead to the estimate

$$\begin{aligned}
 (iii) &= 2 \cdot (iv) \leq 2 \cdot 2C_f|V| \operatorname{ess\,sup}_{|x-y|<\delta, v} \int_0^t C_K \sum_{r=1}^{R-1} \mathbb{1}_{(x-vs, y-vs]}(a_r) \, ds \\
 &\leq 4C_f|V|C_K(R-1)\delta \leq \frac{\varepsilon}{2} e^{-2C_K|V|T}.
 \end{aligned} \tag{42}$$

In summary, Gronwall's lemma yields

$$\operatorname{ess\,sup}_{|x-y|<\delta, v} |f(t, x, v) - f(t, y, v)| \leq \varepsilon e^{-2C_K|V|(T-t)} \leq \varepsilon.$$

□

Again, semigroup theory shows existence of the adjoint equation (10) with corresponding bounds.

Lemma B.2. *Let $h \in L^1((0, T); L^\infty(V; L^1(\mathbb{R})))$, $\psi \in L^1(\mathbb{R})$ and let (12) hold. Then the equation*

$$\begin{aligned}
 -\partial_t g - v \cdot \nabla_x g &= \alpha \tilde{\mathcal{L}}(g) - \sigma g + h, \\
 g(t = T) &= \psi(x)
 \end{aligned} \tag{43}$$

with $\alpha \in \{0, 1\}$ and $\tilde{\mathcal{L}}(g) := \int K(x, v', v) g(x, t, v') \, dv'$ and $\sigma(x, v) := \int K(x, v', v) \, dv'$ has a mild solution

$$g \in C^0([0, T]; L^\infty(V; L^1(\mathbb{R}))) \tag{44}$$

that satisfies

$$\|g(t)\|_{L^\infty(V; L^1(\mathbb{R}))} \leq e^{(1+\alpha)|V|C_K(T-t)} \left(\|\psi\|_{L^1(\mathbb{R})} + \int_0^{T-t} \max_v \|h(T-s, v)\|_{L^1(\mathbb{R})} \, ds \right). \tag{45}$$

If, additionally, $h \in L^\infty([0, T] \times V; L^1(\mathbb{R}))$, then

$$\begin{aligned}
 & \|g(t)\|_{L^\infty(V; L^1(\mathbb{R}))} \\
 & \leq e^{(1+\alpha)|V|C_K(T-t)} \|\psi\|_{L^1(\mathbb{R})} + \frac{e^{(1+\alpha)|V|C_K(T-t)} - 1}{(1+\alpha)|V|C_K} \operatorname{ess\,sup}_{t, v} \|h(t, v)\|_{L^1(\mathbb{R})}.
 \end{aligned} \tag{46}$$

Proof. Repeating the arguments in the proof of Lemma B.1, semigroup theory yields the existence of a mild solution

$$g(t) = S(T-t)\psi + \int_0^{T-t} S(T-t-s)h(T-s) \, ds$$

for the semigroup $S(t)$ generated by the operator $v \cdot \nabla_x + \alpha \tilde{\mathcal{L}} - \sigma$ with $\|S(t)\| \leq e^{(1+\alpha)|V|C_K t}$. This yields (45) and (46). □

C Proof of Lemma 3.7-3.8

In this section, we provide the proof for the two Lemmas in section 3.2. In particular, Lemma 3.7 discusses the smallness of the first term in (28).

Proof for Lemma 3.7. By the assumption on the initial data and Corollary B.1 b), f is uniformly continuous in x , uniformly in v, t . For $n = 0$, the boundedness (29) is a consequence of the explicit representation

$$\bar{g}_0(t, x, v_0) = e^{-\int_0^{T-t} \sigma(x+v_0\tau, v_0) d\tau} (\mu_2^\eta - \mu_1^\eta)(x + v_0(T-t)) \quad (47)$$

together with the step function shape (3) of K , the continuity of f and our assumptions: Write $p_0(t, x, v_0, v') := f(x, t, v')e^{-\int_0^{T-t} \sigma(x+v_0\tau, v_0) d\tau}$ and assume without loss of generality $x_1 \geq x_2$, then

$$\begin{aligned} & \int_{I_r} f' \bar{g}_0 dx \\ &= \int_{I_r} p_0(t, x, v_0, v') (\mu_2^\eta - \mu_1^\eta)(x + v_0(T-t)) dx \\ &= - \int_{a_{r-1}-(x_1-x_2)}^{a_{r-1}} p_0(t, x + (x_1 - x_2), v_0, v') \mu_2^\eta(x + v_0(T-t)) dx \\ & \quad + \int_{a_r-(x_1-x_2)}^{a_r} p_0(t, x, v_0, v') \mu_2^\eta(x + v_0(T-t)) dx \\ & \quad + \int_{a_{r-1}}^{a_r-(x_1-x_2)} (p_0(t, x, v_0, v') - p_0(t, x + (x_1 - x_2), v_0, v')) \mu_2^\eta(x + v_0(T-t)) dx, \end{aligned}$$

where we used the substitution $x \rightarrow x - (x_1 - x_2)$ for the integration domain of test function $\mu_1^\eta(x) = \mu_2^\eta(x - (x_1 - x_2))$. By uniform continuity and boundedness of f a similar argumentation as in (42) shows that $p_0(t, x, v_0, v')$ is uniformly continuous in x , uniformly in t, v_0, v' , as well. The corresponding threshold from the epsilon-delta criterion is denoted by $\delta_{p_0}(\varepsilon)$. Then, for $0 \leq |x_1 - x_2| < \delta_0(\varepsilon) := \min(\min_r |a_r - x_2| - T - \eta_0, \delta_{p_0}(\varepsilon))$, the first two integrals vanish, because $\mu_2^\eta(x + v_0(T-t)) = 0$ for all x in the integration domain. We are left with

$$\begin{aligned} \left| \int_{I_r} f' \bar{g}_0 dx \right| &\leq \int_{a_{r-1}}^{a_r-(x_1-x_2)} |p_0(t, x, v_0, v') - p_0(t, x + (x_1 - x_2), v_0, v')| \mu_2^\eta(x + v_0(T-t)) dx \\ &\leq \varepsilon \int_{\mathbb{R}} \mu_2^\eta(x + v_0(T-t)) dx = \varepsilon. \end{aligned}$$

For $n \geq 1$, source iteration shows that the solution to (26) has the form

$$\begin{aligned} \bar{g}_n(t, x, v_0) &= \int_0^{T-t} \int_V \dots \int_0^{T-t-\sum_{j=0}^{n-2} s_j} \int_V p_n(t, x, (v_i)_{i=0, \dots, n}, (s_j)_{j=0, \dots, n-1}) \cdot \\ & \quad (\mu_2 - \mu_1) \left(x + \sum_{l=0}^{n-1} v_l s_l + v_n \left(T - t - \sum_{l=0}^{n-1} s_l \right) \right) dv_n ds_{n-1} \dots dv_1 ds_0. \end{aligned}$$

The function p_n is bounded $0 \leq p_n \leq C_K^n$ and satisfies

$$\int_0^T |p_n(t, x + v_n t, (v_i)_i, (s_j)_j) - p_n(t, y + v_n t, (v_i)_i, (s_j)_j)| dt < \varepsilon$$

for $|x - y| < \delta_{p_n}(\varepsilon)$, uniformly in $(v_i)_i, (s_j)_j$. The assertion then follows in analogy to the case $n = 0$. \square

Lemma 3.8 argues the smallness of the second term in (28). We provide the proof below. It is a consequence of the smallness of $\bar{g}_{>N}$ by Lemma B.2 and the boundedness of f .

Proof for Lemma 3.8. Application of lemma B.2 to $g = \bar{g}_{>N}$, $h = \tilde{\mathcal{L}}\bar{g}_N$, $\alpha = 1$ and $\psi = 0$ yields

$$\begin{aligned} \max_v \int_{\mathbb{R}} |\bar{g}_{>N}(t)| dx &\leq e^{2C_K|V|(T-t)} \int_0^{T-t} \sup_v \|\tilde{\mathcal{L}}(\bar{g}_N)(T-s, v)\|_{L^1(\mathbb{R})} ds \\ &\leq |V|C_K(T-t)e^{2C_K|V|(T-t)} \operatorname{ess\,sup}_{s,v} \|\bar{g}_N(s, x, v)\|_{L^1(\mathbb{R})}. \end{aligned}$$

Now, application of the same lemma to the evolution equation (26) for g_n , $n = 1, \dots, N$, shows

$$\operatorname{ess\,sup}_{t,v} \int_{\mathbb{R}} |\bar{g}_n| \, dx \leq (e^{C_K|V|T} - 1) \operatorname{ess\,sup}_{s,v} \int_{\mathbb{R}} |\bar{g}_{n-1}(s, x, v)| \, dx.$$

The boundedness of f in (40) and repeated application of the above estimate lead to

$$\begin{aligned} & \left| \int_0^T \max_v \int_{\mathbb{R}} f' \bar{g}_{>N} \, dx \, dt \right| \\ & \leq \frac{T^2}{2} |V| C_K C_\phi e^{2|V|C_K T} (e^{C_K|V|T} - 1)^N \operatorname{ess\,sup}_{s,v} \int_{\mathbb{R}} |\bar{g}_0(s, x, v)| \, dx \\ & \leq \frac{T^2}{2} |V| C_K C_\phi e^{2|V|C_K T} (e^{C_K|V|T} - 1)^N \operatorname{ess\,sup}_{s,v} \int_{\mathbb{R}} |(\mu_2^\eta - \mu_1^\eta)(x + vs)| \, dx \\ & \leq T^2 |V| C_K C_\phi e^{2|V|C_K T} (e^{C_K|V|T} - 1)^N C_\mu, \end{aligned}$$

where $|\bar{g}_0(s, x, v)| \leq |(\mu_2^\eta - \mu_1^\eta)(x + vs)|$ can be observed from the explicit formula for \bar{g}_0 in (47). \square

D Proof of Lemmas in Section 4

We provide proofs for Lemma 4.5-4.6 in this section.

Proof of Lemma 4.5. Use the explicit representations

$$g_1^{(0)}(t, x, v) = e^{-(T-t)\sigma_1(v)} \mu_1(x + v(T-t)), \quad (48)$$

$$f^{(0)}(t, x, v) = e^{-t\sigma_1(v)} \phi(x - vt) \quad (49)$$

with $\sigma_1(v) = \int_V K_1(v', v) \, dv'$ and set without loss of generality $c_1 = 0$. Since $f^{(0)}|_{I_1} = f_1^{(0)}$ in the notation of the proof of Proposition 4.1, one obtains for $(v, v') = (+1, -1)$

$$\begin{aligned} & \int_0^T \int_{I_1} f^{(0)}(v') (g_1^{(0)}(v') - g_1^{(0)}(v)) \, dx \, dt \\ & = \int_0^T \int_{I_1} e^{-t\sigma_1(v')} \phi_1(x - v't) (e^{-(T-t)\sigma_1(v')} \mu_1(x + v'(T-t)) \\ & \quad - e^{-(T-t)\sigma_1(v)} \mu_1(x + v(T-t))) \, dx \, dt \\ & \geq e^{-T\sigma_1(-1)} T \int_{a_0+T}^{a_1} \phi_1(x) \mu_1(-T+x) \, dx - \int_{T-\frac{d_\mu+d}{2}}^T \int_{I_1} \phi_1(x) \mu_1(-T+x) \, dx \, dt \\ & \geq e^{-TC_K|V|} TC_{\phi\mu} - \frac{d_\mu + d}{2} C_{\phi\mu}, \end{aligned}$$

where the first inequality is due to the fact that $\phi_1(x - v't) \mu_1(x + v(T-t)) = \phi_1(x+t) \mu_1(x + (T-t)) \neq 0$ only for $x \in [-t-d, -t+d] \cap [-2T+t-d_\mu, -2T+t+d_\mu] \subset I_1$ which is empty for $t \leq T - \frac{d_\mu+d}{2}$.

For $(v', v) = (-1, +1)$, instead, we obtain

$$\begin{aligned} & \left| \int_0^T \int_{I_1} f^{(0)}(v) (g_1^{(0)}(v) - g_1^{(0)}(v')) \, dx \, dt \right| \\ & = \left| \int_0^T \int_{I_1} e^{-t\sigma_1(v)} \phi_1(x - vt) (e^{-(T-t)\sigma_1(v)} \mu_1(x + v(T-t)) \right. \\ & \quad \left. - e^{-(T-t)\sigma_1(v')} \mu_1(x + v'(T-t))) \, dx \, dt \right| \\ & \leq C_{\phi\mu} \frac{d + d_\mu}{2} \end{aligned}$$

since

- $\phi_1(x - vt) \mu_1(x + v(T-t)) = \phi_1(x-t) \mu_1(x + T-t)$ vanishes, as its support $[t-d, t+d] \cap [-2T+t-d_\mu, -2T+t+d_\mu] = \emptyset$ is empty by construction of $T > d \geq d_\mu$ and

- the support $[t-d, t+d] \cap [-t-d_\mu, -t+d_\mu]$ of $\phi_1(x-vt)\mu_1(x+v'(T-t)) = \phi_1(x-t)\mu_1(x-(T-t))$ is non-empty only for $t \leq \frac{d+d_\mu}{2}$.

Since $e^{-TC_K|V|} - \frac{d_\mu+d}{T} > 0$ by assumption, this proves the assertion. □

To show inequality (37) in Lemma 4.6, decompose for some $N \in \mathbb{N}$ to be determined later

$$\begin{aligned} S = & \sum_{\substack{n,k=0 \\ n+k \geq 1}}^N \int_0^T \int_{I_1} f^{(k)}(v')(g_1^{(n)}(v') - g_1^{(n)}(v)) dx dt \\ & + \int_0^T \int_{I_1} f(v')(g_1^{(>N)}(v') - g_1^{(>N)}(v)) dx dt \\ & + \sum_{n=0}^N \int_0^T \int_{I_1} f^{(>N)}(v')(g_1^{(n)}(v') - g_1^{(n)}(v)) dx dt, \end{aligned} \quad (50)$$

where $g_1^{(n)}$ and $g_1^{(>N)}$ solve (26) and (27) respectively and $f^{(k)}$ are solutions to

$$\begin{aligned} \partial_t f^{(k)} - v \cdot \nabla_x f^{(k)} &= \mathcal{L}(f^{(k-1)}) - \sigma f^{(k)}, \\ f^{(k)}(t=0, x, v) &= 0, \end{aligned}$$

with $\mathcal{L}(h) := \int_V K(v, v')h(t, x, v') dv'$, and $f^{(>N)}$ satisfies

$$\begin{aligned} \partial_t f^{(>N)} - v \cdot \nabla_x f^{(>N)} &= \mathcal{L}(f^{(N)} + f^{(>N)}) - \sigma f^{(>N)}, \\ f^{(>N)}(t=0, x, v) &= 0. \end{aligned}$$

Each part of S in representation (50) is estimated separately in the subsequent three lemmas.

Lemma D.1. *In the setting of proposition 4.2,*

$$\begin{aligned} \left| \int_0^T \int_{I_1} f^{(k)}(v')(g_1^{(n)}(v') - g_1^{(n)}(v)) dx dt \right| &\leq 2 \max_{v, v'} \int_0^T \int_{I_1} f^{(k)}(v')g_1^{(n)}(v) dx dt \\ &\leq 2(C_K|V|)^{n+k} T^{n+k+1} C_{\phi\mu} \end{aligned}$$

Proof. Source iteration

$$\begin{aligned} g_1^{(n)}(t, x, v_0) &= \int_0^{T-t} \int_V e^{-s_0\sigma(v_0)} K_1(\hat{v}_1, v_0) g_1^{(n-1)}(t+s_0, x+v_0s_0, \hat{v}_1) d\hat{v}_1 ds_0 \\ &\leq |V| \int_0^{T-t} e^{-s_0\sigma(v_0)} K_1(v_1, v_0) g_1^{(n-1)}(t+s_0, x+v_0s_0, v_1) ds_0, \\ f^{(k)}(t, x, v_0) &= \int_0^t \int_V e^{-s_0\sigma(v_0)} K(v_0, \hat{v}_1) f^{(k-1)}(t-s_0, x-v_0s_0, \hat{v}_1) d\hat{v}_1 ds_0 \\ &\leq |V| \int_0^t e^{-s_0\sigma(v_0)} K(v_0, v_1) f^{(k-1)}(t-s_0, x-v_0s_0, v_1) ds_0, \end{aligned}$$

where $v_1 = -v_0$, together with the explicit formulas (48)–(49) leads to estimates

$$\begin{aligned} 0 \leq g_1^{(n)}(x, t, v_0) &\leq (C_K|V|)^n \int_0^{T-t} \dots \int_0^{T-t-\sum_{i=0}^{n-2} s_i} \mu_1 \left(x + \sum_{i=0}^{n-1} v_i s_i + v_n \left(T-t - \sum_{i=0}^{n-1} s_i \right) \right) \\ &\quad ds_{n-1} \dots ds_0, \\ 0 \leq f^{(k)}(x, t, v_0) &\leq (C_K|V|)^k \int_0^t \dots \int_0^{t-\sum_{i=0}^{k-2} s_i} \phi \left(x - \sum_{i=0}^{k-1} v_i s_i + v_k \left(t - \sum_{i=0}^{k-1} s_i \right) \right) ds_{k-1} \dots ds_0. \end{aligned} \quad (51)$$

Using again $f^{(k)}|_{I_1} = f_1^{(k)}$ with initial condition ϕ_1 in the notation of the proof of Porposition 4.1, this proves

$$\begin{aligned} \left| \int_0^T \int_{I_1} f^{(k)}(v')(g_1^{(n)}(v') - g_1^{(n)}(v)) dx dt \right| &\leq 2 \max_{v, v'} \int_0^T \int_{I_1} f_1^{(k)}(v')g_1^{(n)}(v) dx dt \\ &\leq 2(C_K|V|)^{n+k} T^{n+k+1} C_{\phi\mu}. \end{aligned}$$

□

The following bound for the second summand in (50) is obtained in analogy to Lemma 3.8.

Lemma D.2. *In the setting of Proposition 4.2,*

$$\begin{aligned} & \max_v \left| \iint f(v')(g_1^{(>N)}(v') - g_1^{(>N)}(v)) dx dt \right| \\ & \leq 4T^2 |V| C_K C_\phi e^{2|V|C_K T} (e^{C_K|V|T} - 1)^N \bar{C}_\mu d_\mu =: C'(T) (e^{C_K|V|T} - 1)^N \end{aligned}$$

For the third term in (50), one establishes the following bound.

Lemma D.3. *In the setting of Proposition 4.2,*

$$\begin{aligned} & \max_v \left| \iint f^{(>N)}(v')(g^{(n)}(v') - g^{(n)}(v)) dx dt \right| \\ & \leq 4|V| C_K T^2 e^{2|V|C_K T} (e^{C_K|V|T} - 1)^N C_\phi (C_K|V|T)^n \bar{C}_\mu d_\mu \\ & =: C''(T) (e^{C_K|V|T} - 1)^N (C_K|V|T)^n \end{aligned}$$

Proof. An estimate for $f^{(>N)}$ can be derived analogously as the estimate for $\bar{g}_{>N}$ in Lemma 3.8 from Lemma B.1

$$\|f^{(>N)}\|_{L^\infty([0,T] \times \mathbb{R} \times V)} \leq |V| C_K T e^{2|V|C_K T} (e^{C_K|V|T} - 1)^N C_\phi.$$

Together with (51), this proves the lemma. □

Lemma 4.6 can now be assembled from the previous lemmas.

Proof of Lemma 4.6. Lemmas D.1, D.2 and D.3 yield the (v, v') independent bound

$$\begin{aligned} |S| & \leq 2C_{\phi\mu} T \sum_{\substack{n,k=0 \\ n+k \geq 1}}^N (C_K|V|T)^{n+k} + (e^{C_K|V|T} - 1)^N \left(C'(T) + C''(T) \sum_{n=0}^N (C_K|V|T)^n \right) \\ & \leq 4C_{\phi\mu} T \frac{C_K|V|T}{(1 - C_K|V|T)^2} + (e^{C_K|V|T} - 1)^N \left(C'(T) + C''(T) \frac{1}{1 - C_K|V|T} \right) \\ & =: 4C_{\phi\mu} T \frac{C_K|V|T}{(1 - C_K|V|T)^2} + (e^{C_K|V|T} - 1)^N C(T). \end{aligned}$$

Because $e^{C_K|V|T} - 1 < 1$ due to the assumption $T < (1 - \delta) \frac{0.09}{C_K|V|}$, the second term in the last line becomes arbitrarily small for large $N \in \mathbb{N}$, which shows that $|S|$ is in fact bounded by the first term. □

References

- H.C. Berg. *Random Walks in Biology*. Princeton paperbacks. Princeton University Press, 1993. ISBN 9780691000640. URL <https://books.google.com/books?id=DjdgXGLoJY8C>.
- Casimir Emako, Charlene Gayraud, Axel Buguin, Luís Neves de Almeida, and Nicolas Vauchelet. Traveling pulses for a two-species chemotaxis model. *PLOS Computational Biology*, 12(4):1–22, 04 2016. doi:10.1371/journal.pcbi.1004843. URL <https://doi.org/10.1371/journal.pcbi.1004843>.
- J. Saragosti, V. Calvez, N. Bournaveas, B. Perthame, A. Buguin, and P. Silberzan. Directional persistence of chemotactic bacteria in a traveling concentration wave. *Proceedings of the National Academy of Sciences*, 108(39):16235–16240, 2011. doi:10.1073/pnas.1101996108. URL <https://www.pnas.org/doi/abs/10.1073/pnas.1101996108>.
- Jonathan Saragosti, Vincent Calvez, Nikolaos Bournaveas, Axel Buguin, Pascal Silberzan, and Benoît Perthame. Mathematical description of bacterial traveling pulses. *PLOS Computational Biology*, 6(8):1–12, 08 2010. doi:10.1371/journal.pcbi.1000890. URL <https://doi.org/10.1371/journal.pcbi.1000890>.
- He Li, Xia qing Shi, Mingji Huang, Xiao Chen, Minfeng Xiao, Chenli Liu, Hugues Chaté, and H. P. Zhang. Data-driven quantitative modeling of bacterial active nematics. *Proceedings of the National Academy of Sciences*, 116(3): 777–785, 2019. doi:10.1073/pnas.1812570116.
- B. Davison and J.B. Sykes. *Neutron Transport Theory*. International series of monographs on physics. Clarendon Press ; [Oxford University Press], 1958.

- George B. Rybicki and Alan P. Lightman. Radiative Processes in Astrophysics. WILEY-VCH, 1986.
- C. Cercignani. The Boltzmann Equation and Its Applications. Applied Mathematical Sciences. Springer New York, 2012. ISBN 9781461210399. URL <https://books.google.de/books?id=0cTcBwAAQBAJ>.
- Hans Othmer, S Dunbar, and W Alt. Models of dispersal in biological systems. Journal of mathematical biology, 26: 263–98, 02 1988. doi:10.1007/BF00277392.
- Jake Taylor-King, E Loon, Gabriel Rosser, and Stephen Chapman. From birds to bacteria: Generalised velocity jump processes with resting states. Bulletin of mathematical biology, 77:1213–1236, 07 2014. doi:10.1007/s11538-015-0083-7.
- Giacomo Albi, Elisa Calzola, and Giacomo Dimarco. A data-driven kinetic model for opinion dynamics with social network contacts, 2023.
- J. Carrillo, M Fornasier, Jesús Rosado, and Giuseppe Toscani. Asymptotic flocking dynamics for the kinetic cucker–smale model. SIAM Journal on Mathematical Analysis, 42, 05 2009. doi:10.1137/090757290.
- Weiqi Chu, Qin Li, and Mason A. Porter. Inference of interaction kernels in mean-field models of opinion dynamics, 2022.
- Sebastien Motsch and Eitan Tadmor. Heterophilious dynamics enhances consensus. SIAM Review, 56(4):577–621, 2014. doi:10.1137/120901866.
- Giuseppe Toscani. Kinetic models of opinion formation. Commun. Math. Sci., 4:481–496, 09 2006. doi:10.4310/CMS.2006.v4.n3.a1.
- Guillaume Bal, Ian Langmore, and Francois Monard. Inverse transport with isotropic sources and angularly averaged measurements. Inverse Problems and Imaging, 1:23–42, 02 2008. doi:10.3934/ipi.2008.2.23.
- M Choulli and P Stefanov. Reconstruction of the coefficients of the stationary transport equation from boundary measurements. Inverse Problems, 12(5):L19–L23, oct 1996. doi:10.1088/0266-5611/12/5/001.
- Ru-Yu Lai, Qin Li, and Gunther Uhlmann. Inverse problems for the stationary transport equation in the diffusion scaling. SIAM Journal on Applied Mathematics, 79(6):2340–2358, 2019. doi:10.1137/18M1207582.
- Qin Li and Weiran Sun. Applications of kinetic tools to inverse transport problems. Inverse Problems, 36(3):035011, Feb 2020.
- Simon R Arridge and John C Schotland. Optical tomography: forward and inverse problems. Inverse Problems, 25(12): 123010, dec 2009. doi:10.1088/0266-5611/25/12/123010. URL <https://dx.doi.org/10.1088/0266-5611/25/12/123010>.
- Ke Chen, Qin Li, and Jian-Guo Liu. Online learning in optical tomography: a stochastic approach. Inverse Problems, 34(7):075010, may 2018. doi:10.1088/1361-6420/aac220.
- Herbert Egger and Matthias Schlottbom. Numerical methods for parameter identification in stationary radiative transfer. Computational Optimization and Applications, page 67–83, 11 2013. doi:10.1007/s10589-014-9657-9.
- Kernel Prieto and Oliver Dorn. Sparsity and level set regularization for diffuse optical tomography using a transport model in 2d. Inverse Problems, 33(1):014001, nov 2016. doi:10.1088/0266-5611/33/1/014001.
- Kui Ren. Recent developments in numerical techniques for transport-based medical imaging methods. Communications in Computational Physics, 8(1):1–50, 2010. ISSN 1991-7120. doi:<https://doi.org/10.4208/cicp.220509.200110a>.
- Hannah Jeckel, Eric Jelli, Raimo Hartmann, Praveen K. Singh, Rachel Mok, Jan Frederik Totz, Lucia Vidakovic, Bruno Eckhardt, Jörn Dunkel, and Knut Drescher. Learning the space-time phase diagram of bacterial swarm expansion. Proceedings of the National Academy of Sciences, 116(5):1489–1494, 2019. doi:10.1073/pnas.1811722116.
- H. P. Zhang, Avraham Be’er, E.-L. Florin, and Harry L. Swinney. Collective motion and density fluctuations in bacterial colonies. Proceedings of the National Academy of Sciences, 107(31):13626–13630, 2010. doi:10.1073/pnas.1001651107.
- Kathrin Hellmuth, Christian Klingenberg, Qin Li, and Min Tang. Kinetic chemotaxis tumbling kernel determined from macroscopic quantities, 2022.
- Roseanne M. Ford and Douglas A. Lauffenburger. Measurement of bacterial random motility and chemotaxis coefficients: II. application of single-cell-based mathematical model. Biotechnology and Bioengineering, 37(7):661–672, 1991. doi:<https://doi.org/10.1002/bit.260370708>.
- Andrea Giometto, Florian Altermatt, Amos Maritan, Roman Stocker, and Andrea Rinaldo. Generalized receptor law governs phototaxis in the phytoplankton euglena gracilis. Proceedings of the National Academy of Sciences, 112(22):7045–7050, 2015. ISSN 0027-8424. doi:10.1073/pnas.1422922112.

- Mehdi Salek, Francesco Carrara, Vicente Fernandez, Jeffrey Guasto, and Roman Stocker. Bacterial chemotaxis in a microfluidic t-maze reveals strong phenotypic heterogeneity in chemotactic sensitivity. *Nature Communications*, 10, 04 2019. doi:10.1038/s41467-019-09521-2.
- R. T. Tranquillo, S. H. Zigmond, and D. A. Lauffenburger. Measurement of the chemotaxis coefficient for human neutrophils in the under-agarose migration assay. *Cell Motility*, 11(1):1–15, 1988. doi:10.1002/cm.970110102.
- Oliver Pohl, Marius Hintsche, Zahra Alirezaeizanjani, Maximilian Seyrich, Carsten Beta, and Holger Stark. Inferring the chemotactic strategy of *p. putida* and *e. coli* using modified kramers-moyal coefficients. *PLOS Computational Biology*, 13(1):1–24, 01 2017. doi:10.1371/journal.pcbi.1005329.
- Maximilian Seyrich, Zahra Alirezaeizanjani, Carsten Beta, and Holger Stark. Statistical parameter inference of bacterial swimming strategies. *New Journal of Physics*, 20(10):103033, oct 2018. doi:10.1088/1367-2630/aae72c.
- Herbert Egger, Jan-Frederik Pietschmann, and Matthias Schlottbom. Identification of chemotaxis models with volume-filling. *SIAM Journal on Applied Mathematics*, 75(2):275–288, 2015. doi:10.1137/140967222.
- Katherine Fister and Maeve Mccarthy. Identification of a chemotactic sensitivity in a coupled system. *Mathematical medicine and biology : a journal of the IMA*, 25:215–32, 09 2008. doi:10.1093/imammmb/dqn015.
- Stephen J. Wright and Benjamin Recht. *Optimization for Data Analysis*. Cambridge University Press, 2022. doi:10.1017/9781009004282.
- Boris Polyak and Pavel Shcherbakov. Lyapunov functions: An optimization theory perspective. *IFAC-PapersOnLine*, 50(1):7456–7461, 2017. ISSN 2405-8963. doi:https://doi.org/10.1016/j.ifacol.2017.08.1513. 20th IFAC World Congress.
- Rosa Ferrentino and Carmine Boniello. On the well-posedness for optimization problems: A theoretical investigation. *Applied Mathematics*, 10:19–38, 01 2019. doi:10.4236/am.2019.101003.
- Roger A. Horn and Charles R. Johnson. *Matrix Analysis*. Cambridge University Press, 1985. doi:10.1017/CBO9780511810817.
- Francis Filbet and Chang Yang. Numerical simulations of kinetic models for chemotaxis. *SIAM Journal on Scientific Computing*, 36(3):B348–B366, 2014. doi:10.1137/130910208.
- Thomas Apel and Thomas G. Flaig. Crank–nicolson schemes for optimal control problems with evolution equations. *SIAM Journal on Numerical Analysis*, 50(3):1484–1512, 2012. doi:10.1137/100819333.
- Martin Burger and Wolfram Mühlhuber. Iterative regularization of parameter identification problems by sequential quadratic programming methods. *Inverse Problems*, 18(4):943, may 2002. doi:10.1088/0266-5611/18/4/301.
- Eldad Haber, Uri M Ascher, and Doug Oldenburg. On optimization techniques for solving nonlinear inverse problems. *Inverse Problems*, 16(5):1263, oct 2000. doi:10.1088/0266-5611/16/5/309. URL https://dx.doi.org/10.1088/0266-5611/16/5/309.
- Danny Smyl, Tyler N. Tallman, Dong Liu, and Andreas Hauptmann. An efficient quasi-newton method for nonlinear inverse problems via learned singular values. *IEEE Signal Processing Letters*, 28:748–752, 2021. doi:10.1109/LSP.2021.3063622.
- Max D. Gunzburger. *Perspectives in Flow Control and Optimization*. Society for Industrial and Applied Mathematics, 2002. doi:10.1137/1.9780898718720.
- Jun Liu and Zhu Wang. Non-commutative discretize-then-optimize algorithms for elliptic pde-constrained optimal control problems. *Journal of Computational and Applied Mathematics*, 362:596–613, 2019. ISSN 0377-0427. doi:https://doi.org/10.1016/j.cam.2018.07.028.
- Michael Hinze, René Pinnau, Michael Ulbrich, and Stefan Ulbrich. Optimization with pde constraints. In *Mathematical Modelling*, 2008.
- Dung Le. Dynamics of a bio-reactor model with chemotaxis. *Journal of Mathematical Analysis and Applications*, 275 (1):188–207, 2002. ISSN 0022-247X. doi:https://doi.org/10.1016/S0022-247X(02)00313-X.
- Alen Alexanderian. Optimal experimental design for infinite-dimensional bayesian inverse problems governed by pdes: a review. *Inverse Problems*, 37(4):043001, mar 2021. doi:10.1088/1361-6420/abe10c.
- Klaus-Jochen Engel and Rainer Nagel. *One-Parameter Semigroups for Linear Evolution Equations*, volume 63. Springer-Verlag New York, 06 2001. doi:10.1007/s002330010042.